IEEE Access
Multidisciplinary | Rapid Review | Open Access Journal

Received March 31, 2019, accepted May 6, 2019, date of publication May 13, 2019, date of current version May 29, 2019.

Digital Object Identifier 10.1109/ACCESS.2019.2916394

Time Domain Finite Element Method for Maxwell's Equations

ASAD ANEES AND LUTZ ANGERMANN
Institute of Mathematics, Clausthal University of Technology, 38678 Clausthal-Zellerfeld, Germany
Corresponding author: Asad Anees (asad.anees@tu-clausthal.de)

This work was partially supported by the German Academic Exchange Service (DAAD) through a Funding Program under Grant 57129429, and by the Open Access Publishing Fund of the Clausthal University of Technology.

ABSTRACT In this paper, we discuss a time domain finite element method for the approximate solution of Maxwell's equations. A weak formulation is derived for the electric and magnetic fields with appropriate initial and boundary conditions, and the problem is discretized both in space and time. In space, Nédeléc curl-conforming and Raviart–Thomas div-conforming finite elements are used to discretize the electric and magnetic fields, respectively. The backward Euler and symplectic schemes are applied to discretize the problem in time. For this system, we prove an error estimate. In addition, computational experiments are presented to validate the method, the electric and magnetic fields are visualized. The method also allows treating complex geometries of various physical systems coupled to electromagnetic fields in 3D.

INDEX TERMS Backward Euler method, error estimates, Maxwell's equations, time domain finite element methods, simulation, symplectic method, visualization.

I. INTRODUCTION

The solution of Maxwell's equations in the time domain formulation is involved in many engineering and industrial problems, e.g. RF, radar, mixed signal integrated circuits (ICs), diffraction of electromagnetic waves, plasma physics, acoustic or seismic wave propagation, radiation, scattering, environmental and medical imaging, and microwave devices. In the presence of complex media or geometries, finite element methods in either continuous or discontinuous variants are the main numerical approaches. In the literature an abundance of work about convergence analysis, semi-discrete, fully-discrete error estimates, and numerical simulations for the time dependent Maxwell's equations exists. The Galerkin time domain finite element methods (TDFEM) can be grouped into two classes, one class of schemes directly deals with the system of Maxwell's equations, whereas the other class solves the second order wave equations (classical approach).

In the classical approach, second order wave equations or hyperbolic system are obtained either by eliminating the electric or magnetic field from the system of Maxwell's equations. The resulting problems are called electric or magnetic field formulations, respectively. In the literature, a lot of papers have been devoted to the solution of second order wave equations [1]–[15]. In [1], Monk presented semi-discrete error estimates in the energy and $\mathbf{L}^2$ norms by employing Nédeléc curl-conforming elements for the vector wave equations. The paper [2] presents TDFEM for the second order vector wave equations and hyperbolic systems using node-based and edge-based elements. Various numerical experiments were performed to investigate the advantages or disadvantages of the mass lumping scheme. Comparisons of various TDFEM and semi-discrete error estimates are presented in [3] for the electric field hyperbolic equation in anisotropic and inhomogeneous media with respect to test and trial spaces, explicit and implicit formulations. Moreover, the convergence of a fully discrete finite element scheme is analyzed for the second order electric field equation (vector wave equation) in [4], and optimal error estimates are obtained in the $\mathbf{L}^2$ norm. Furthermore, the only simulations of the second order vector wave equation are described in [5], [12], [14], [15]. In the papers [4] and [5], the vector wave equation is discretized by Nédeléc curl-conforming finite elements in space, and second order backward and central finite differences, respectively are used to discretize in time. The scheme described by White and Stowell [5] is second order accurate in space and time.

The associate editor coordinating the review of this manuscript and approving it for publication was Gang Mei.

Edge finite elements (for the magnetic vector potential) in the time domain are presented in [12] to address the problem of inductive and capacitive effects. A TDFEM (curl-curl electric field equation) forward solver transmitting loop is presented in [13] to address for a complex shaped domain. A local time stepping method (LTS) based on explicit Runge-Kutta schemes having arbitrary accuracy in time for wave propagation is demonstrated in [14].

The vector wave equation and magnetic vector potential approaches allow to address the Maxwell's equations in time domain, an easy implementation for analysis, error estimation and simulations. However, the simulation, analysis and error estimation of the wave equation (electric field formulation and magnetic field formulation) cause spurious and non-physical solutions that are linearly raising corresponding to time [6], [9].

In [16]–[32], a number of mixed time domain finite element methods are explained to deal with the system of Maxwell's equations. An abundance of mixed time domain finite element methods for the direct application to Maxwell's system is available, where the electric and magnetic fields are discretized in space by discontinuous and Nédeéc curl-conforming spaces, respectively, see e.g. [16], [20], [22], [23], [29] and [31]. In the work [16], error estimates are demonstrated for a semi-discrete problem, but computational experiments and fully-discrete error estimates are not provided. Both semi-discrete, and fully-discrete (using a Crank-Nicolson discretization) point-wise superconvergence results are obtained for Maxwell's equations in metamaterials for nonuniform cublic and rectangular edge elements in [33]. Lee and Madsen [20] also demonstrated a mixed time domain finite element simulation for Maxwell's equations and employed a explicit leapfrog time integration scheme. A mixed semi-discrete and a fully-discrete error analysis for Maxwell's equations in double negative material are given in [22], but computational experiments were not performed. In [34], a variable time step method for time domain Maxwell's equations is presented. Fully discrete error estimates and computational experiments for Maxwell's equations simultaneously for dispersive and Lorentz metamaterials are presented in [23], [31]. There the temporal discretization is done by means of first order backward finite differences, and computational experiments are performed for 2D situations. Error estimates are also presented in [27], where the problem is discretized in space and time by means of Nédeléc curl-conforming finite elements and backward finite differences, respectively. The scheme is called decoupled or explicit magnetic field scheme and causes spurious solutions. Furthermore, other semi-discrete theoretical and numerical results for the time dependent Maxwell's equation in composite material are presented in [29], where the material parameters ε, μ and σ are 3×3 positive definite matrices depending on the spatial variables.

In [18], [21], [26], [32], [35], time domain finite element methods for Maxwell's equations are discussed using curl-conforming and div-conforming elements for spatial discretization. The $\mathbf{L}^2$ error is estimated for a semi-discrete scheme in [26]. We proposed a splitting approach for the Maxwell's equation that splits the system of Maxwell's equations into two uncoupled system, to deal with ε and μ as matrix function of space (complex material) [36]. The splitting method allows to solve the uncoupled systems independently, and is proved to be stable and convergent at the semi-discrete level. The operator form of uncoupled systems and semi-discrete error estimates are presented in [32], but fully-discrete error estimation and computational experiment are not given in [26], [32], [36]. In [18], semi-discrete and fully-discrete error estimates are obtained from the operator form of the system of Maxwell's equations, and the time discretizations by rational approximations of the exponential function are investigated, but no computational experiments were given. Moreover, the only simulations for the system of Maxwell's equations are given in [21], [35]

In the article [19], the Maxwell's equations are discretized in space by a node-based and edge-based finite element method, and an efficient solver is described both for the frequency and time domain formulations. The paper [24] describes a general way to investigate the stability of temporal discretization schemes such as backward difference, forward difference and central difference methods in electromagnetics. The stability is determined by analyzing the root locus map of a characteristic equation and evaluating the spectral radius of finite element system matrix. Stability properties are given in [3] for simulations of transient electromagnetic phenomena for the Maxwell's equations. In the article [25], time domain finite element methods based on Whitney elements are proposed for solving transient response problems on tetrahedral meshes. One of the proposed schemes is unconditionally stable, another scheme is explicit but does not require matrix inversions. An explicit time domain finite element algorithm is presented for the Maxwell's equations in [30], for complex media in [28] (only numerical result). An energy conserving method for 3D Maxwell's equations is obtained in [37], based on an exponential operator splitting approach.

Many papers have been written about time domain discontinuous Galerkin (TDDG) methods in computational electromagnetics [38]–[49]. Other time domain methods to solve either the Maxwell's equations or the vector wave equation can be found in [50]–[62]. Several books for electromagnetics [63]–[68] are available for analysis and simulation.

The TDFEM proposed in [18], [27], [32], [34], [36] also cause spurious and non-physical solutions because these methods do not figure out quantities from the system of Maxwell's equations directly. It is well known that $\mathbf{H}^1$ conforming finite elements for electromagnetics may result in spurious and non-physical solutions. The degrees of freedom for Nédeléc curl-conforming and Raviart-Thomas div-conforming finite elements are related to the edges and faces of the meshes, respectively, and not to the mesh nodes. These finite elements also avoid the appearance of non-physical, spurious and divergent solutions [69], [70]. These are good reasons to use Nédeléc curl-conforming and Raviart-Thomas

div-conforming finite elements. To date most of contributions have been based on Nédeléc curl-conforming (edge elements) for the time domain solution of Maxwell's equation and a few are using (Nédeléc and Raviart-Thomas) edge and face elements with spurious solutions. The technique of error estimation and simulation we present is motivated by the last three decades works. We demonstrate error estimates for fully discretized Maxwell's equations based on a time domain finite element approach, and simulations using various solvers and visualizations of the computed electric and magnetic fields. In our approach, we deal with the system of Maxwell's equations rather than the second order vector wave equation. Additionally, the electric and magnetic fields figure out directly both in the error estimates and numerical experiments. For simplicity of presentation, the material parameters ε and μ are considered as time independent, piecewise constant scalar functions, but the results can be generalized to more complicated material parameters, e.g. positively definite tensors. The electric and magnetic fields are discretized by Nédeléc curl-conforming and Raviart-Thomas div-conforming finite elements in space, respectively. The properties of these finite elements have been investigated in many articles [71], [72] and [73]. In addition, the problem is discretized in time by backward Euler and sympletic methods. The error analysis of the mixed finite element method for the fully discrete problem is given in the case of only the backward Euler method, and computational results are given in both cases.

Our proposed schemes deal with the system of Maxwell's equations directly in 3D, which cause no spurious solution. Fully-discrete error estimates and simulation results with visualizations of the electromagnetic quantities are given. Similar results for fully-discrete error estimation could be obtained also for our previous results about the decoupled Maxwell's equations [32], [36]. These are intermediate results that provide a starting point for the development and theoretical-numerical investigation of TDFEM for nonlinear problems in optics and photonics. These include energy-conserving methods in 3D.

To begin with the problem formulation, let $\Omega \subset \mathbb{R}^3$ be a simply connected domain with a smooth boundary Γ and unit outward normal $\mathbf{n}$. The symbols $\mathbf{E} = \mathbf{E}(\mathbf{x}, t)$ and $\mathbf{H} = \mathbf{H}(\mathbf{x}, t)$ denote the electric and magnetic field intensities respectively, where the time variable t belongs to some finite interval $(0, T)$, $0 < T < \infty$. Given a current density function $\mathbf{J} = \mathbf{J}(\mathbf{x}, t)$, specifying the applied current, Maxwell's equations state that

$$\varepsilon \mathbf{E}_t - \nabla \times \mathbf{H} = \mathbf{J} \text{ in } \Omega \times (0, T), \tag{1}$$

$$\mu \mathbf{H}_t + \nabla \times \mathbf{E} = 0 \text{ in } \Omega \times (0, T). \tag{2}$$

The material parameters ε and μ do not depend on time and are piecewise constant. In addition, there exist positive constants $\varepsilon_{\min}, \varepsilon_{\max}, \mu_{\min}, \mu_{\max}$ such that, for all $\mathbf{x} \in \Omega$,

$$0 < \varepsilon_{\min} \leq \varepsilon(\mathbf{x}) \leq \varepsilon_{\max} < \infty,$$
$$0 < \mu_{\min} \leq \mu(\mathbf{x}) \leq \mu_{\max} < \infty.$$

A perfect conducting boundary condition on Ω is assumed, that is,

$$\mathbf{n} \times \mathbf{E} = 0 \quad \text{on } \Gamma \times (0, T).$$

Finally, initial conditions have to be specified so that

$$\mathbf{E}(\mathbf{x}, 0) = \mathbf{E}_0(\mathbf{x}) \quad \text{and } \mathbf{H}(\mathbf{x}, 0) = \mathbf{H}_0(\mathbf{x}) \text{ for all } \mathbf{x} \in \Omega, \tag{3}$$

where $\mathbf{E}_0$ and $\mathbf{H}_0$ are given functions on Γ, and $\mathbf{H}_0$ satisfies

$$\nabla \cdot (\mu \mathbf{H}_0) = 0 \quad \text{in } \Omega, \ \mathbf{H}_0 \cdot \mathbf{n} = 0 \ \text{ on } \Gamma.$$

We assume that the solution $(\mathbf{E}, \mathbf{H})$ of the system $(1) - (3)$ exists and is unique, for details see [74]. The Maxwell's equations with piecewise constant coefficient have been investigated in [16], [75].

The paper is structured as follows. The next section gives an overview over the basic function spaces and notation. Section III describes the weak formulation and an error estimate for the backward Euler semi-discrete method (Rothe method). The spatial discretization is discussed in Section IV. In Section V we describe and investigate the full discretization. Finally Section VI presents a collection of numerical examples.

II. SPACES AND NOTATION

For a real number $p \geq 1$, the space $L^p(\Omega)$ consists of equivalence classes of Lebesgue-measurable functions $u : \Omega \to \mathbb{R}$ such that

$$\int_\Omega |u|^p \, d\mathbf{x} < \infty.$$

If $u \in L^p(\Omega)$, we define its $L^p(\Omega)$-norm as follows :

$$\|u\|_{L^p(\Omega)} = \left\{ \int_\Omega |u(\mathbf{x})|^p \, d\mathbf{x} \right\}^{1/p}.$$

Furthermore, the space $L^\infty(\Omega)$ consists of the equivalence classes of essentially bounded measurable functions $u : \Omega \to \mathbb{R}$ equipped with the norm

$$\|u\|_{L^\infty(\Omega)} = \operatorname*{ess\,sup}_{\mathbf{x} \in \Omega} |u(\mathbf{x})|.$$

The analogous spaces of vector fields $\mathbf{u} : \Omega \to \mathbb{R}^3$ are denoted by $\mathbf{L}^p(\Omega) := [L^p(\Omega)]^3$.

In what follows we have to deal with weighted function spaces. Given a weight $\omega : \Omega \to \mathbb{R}$, where the values of ω are positive a.e. on Ω, we define a weighted inner product and a weighted norm by

$$(\mathbf{u}, \mathbf{v})_\omega := \int_\Omega \omega \, \mathbf{u} \cdot \mathbf{v} \, d\mathbf{x} \quad \text{and,}$$
$$\|\mathbf{u}\|_\omega := \|\mathbf{u}\|_{\mathbf{L}^2_\omega(\Omega)} := \sqrt{(\mathbf{u}, \mathbf{u})_\omega},$$

and the space $\mathbf{L}^2_\omega(\Omega)$ consists of vector fields $\mathbf{u} : \Omega \to \mathbb{R}^3$ with Lebesgue-measurable components and such that

$$\|\mathbf{u}\|_\omega < \infty.$$

In the case $\omega = 1$, the subscript is omitted.

As transient problems are addressed, we will work with functions that depend on time and have values in certain Banach spaces. If $\mathbf{u} = \mathbf{u}(\mathbf{x}, t)$ is a vector field of the space variable $\mathbf{x}$ and the time variable t, it is suitable to separate these variables in such a way that $\mathbf{u}(t) = \mathbf{u}(\cdot, t)$ is considered as a function of t with values in a Banach space, say X, with the norm $\|\cdot\|_X$. That is, for any $t \in (0, T)$, the mapping $\mathbf{x} \mapsto \mathbf{u}(\mathbf{x}, t)$ is interpreted as a parameter-dependent element $\mathbf{u}(t)$ of X. In this sense we will write $\mathbf{E}(t) = \mathbf{E}(\cdot, t)$, $\mathbf{H}(t) = \mathbf{H}(\cdot, t)$ and so on.

The space $\mathbf{C}^m(0, T, X)$, $m \in \mathbb{N} \cup \{0\}$, consists of all continuous functions $\mathbf{u} : (0, T) \to X$ that have continuous derivatives up to order m on $(0, T)$. It is equipped with the norm

$$\sum_{j=0}^{m} \sup_{t\in(0,T)} \|\mathbf{u}^{(j)}(t)\|_X.$$

For the sake of consistency in the notation we will write $\mathbf{C}(0, T, X) := \mathbf{C}^0(0, T, X)$.

The space $\mathbf{L}^p(0, T, X)$ with $1 \le p < \infty$ contains (equivalent classes of) strongly measurable functions $\mathbf{u} : (0, T) \to X$ such that

$$\int_0^T \|\mathbf{u}(t)\|_X^p \, dt < \infty$$

(for the definition of strongly measurable functions we refer to [76]). The norm on $\mathbf{L}^p(0, T, X)$ is defined by

$$\|\mathbf{u}\|_{\mathbf{L}^p(0,T,X)} := \left\{ \int_0^T \|\mathbf{u}(t)\|_X^p \, dt \right\}^{1/p}.$$

These spaces can be equipped with a weight, too. In particular, we will write

$$\|\mathbf{u}\|_{\mathbf{L}^2(0,T,\mathbf{L}^2_\omega(\Omega))} := \left\{ \int_0^T \int_\Omega |\mathbf{u}(t)|^2 \, \omega \, d\mathbf{x} dt \right\}^{1/2}.$$

Next we introduce the Sobolev spaces of functions with weak spatial derivatives of maximal order $r \in \mathbb{N}$ in $L^p(\Omega)$, where α is a multi-index:

$$W^{r,p}(\Omega) := \left\{ u \in L^p(\Omega) : \ \partial^\alpha u \in L^p(\Omega) \ \forall\, |\alpha| \le r \right\}.$$

For $p \ge 1$, the norms and semi-norms are defined by

$$\|u\|^p_{W^{r,p}(\Omega)} := \sum_{|\alpha|\le r} \int_\Omega \|\partial^\alpha u\|^p \, d\mathbf{x},$$

$$|u|^p_{W^{r,p}(\Omega)} := \sum_{|\alpha|= r} \int_\Omega \|\partial^\alpha u\|^p \, d\mathbf{x}.$$

The modifications for $p = \infty$ are obvious. If $p = 2$, we write $H^r(\Omega) := W^{r,2}(\Omega)$ and $\|\cdot\|_{H^r(\Omega)} := \|\cdot\|_{W^{r,2}(\Omega)}$.

The space $H^1_0(\Omega)$ is defined as the closure of $C^\infty_0(\Omega)$ with respect to the norm $\|\cdot\|_{H^1(\Omega)}$, where $C^\infty_0(\Omega)$ denotes the space of all arbitrarily often differentiable functions with compact support on Ω. It is well known that $H^1_0(\Omega)$ is a closed subspace of $H^1(\Omega)$ and consists of elements u such that $u = 0$ on Γ in the sense of traces [77]. As in the case of the L^p-spaces, we shall write $\mathbf{W}^{r,p}(\Omega) := [W^{r,p}(\Omega)]^3$ and so on.

Furthermore, we need the following Hilbert spaces that are related to the (weak) rotation and divergence operators:

$$\begin{aligned}
\mathbf{H}(\mathrm{curl};\Omega) &:= \{\mathbf{u} \in \mathbf{L}^2(\Omega) : \ \nabla \times \mathbf{u} \in \mathbf{L}^2(\Omega)\},\\
\mathbf{H}_0(\mathrm{curl};\Omega) &:= \{\mathbf{u} \in \mathbf{H}(\mathrm{curl};\Omega) : \ \mathbf{u} \times \mathbf{n}|_\Gamma = 0\},\\
\mathbf{H}(\mathrm{div};\Omega) &:= \{\mathbf{u} \in \mathbf{L}^2(\Omega) : \ \nabla \cdot \mathbf{u} \in \mathbf{L}^2(\Omega)\},\\
\mathbf{H}_0(\mathrm{div};\Omega) &:= \{\mathbf{u} \in \mathbf{H}(\mathrm{div};\Omega) : \ \mathbf{u} \cdot \mathbf{n}|_\Gamma = 0\}.
\end{aligned}$$

These Hilbert spaces are equipped with the norms (resp. induced norms)

$$\begin{aligned}
\|\mathbf{u}\|_{\mathbf{H}(\mathrm{curl};\Omega)} &:= \left\{\|\mathbf{u}\|_0^2 + \|\nabla \times \mathbf{u}\|_0^2\right\}^{1/2},\\
\|\mathbf{u}\|_{\mathbf{H}(\mathrm{div};\Omega)} &:= \left\{\|\mathbf{u}\|_0^2 + \|\nabla \cdot \mathbf{u}\|_0^2\right\}^{1/2}.
\end{aligned}$$

We refer to [73], [75], [78] and [79] for details about these spaces.

III. WEAK FORMULATION

Given $\mathbf{J} \in \mathbf{C}(0, T, \mathbf{L}^2_{\varepsilon^{-1}}(\Omega))$, and the weak solution $(\mathbf{E}, \mathbf{H}) \in \big(\mathbf{C}(0, T, \mathbf{H}_0(\mathrm{curl};\Omega)) \cap \mathbf{C}^1(0, T, \mathbf{L}^2_\varepsilon(\Omega))\big) \times \big(\mathbf{C}(0, T, \mathbf{H}(\mathrm{div};\Omega)) \cap \mathbf{C}^1(0, T, \mathbf{L}^2_\mu(\Omega))\big)$ of the system (1)–(2) satisfies

$$(\varepsilon \mathbf{E}_t, \Psi) - (\mathbf{H}, \nabla \times \Psi) = (\mathbf{J}, \Psi) \quad \forall\, \Psi \in \mathbf{H}_0(\mathrm{curl};\Omega), \tag{4}$$

$$(\mu \mathbf{H}_t, \Phi) + (\nabla \times \mathbf{E}, \Phi) = 0 \quad \forall\, \Phi \in \mathbf{H}(\mathrm{div};\Omega), \tag{5}$$

for $t \in (0, T)$ with the initial conditions (3).

Theorem 1: Let $\mathbf{J} \in \mathbf{C}(0, T, \mathbf{L}^2_{\varepsilon^{-1}}(\Omega))$, *and the solution* $(\mathbf{E}, \mathbf{H}) \in \big(\mathbf{C}(0, T, \mathbf{H}_0(\mathrm{curl};\Omega)) \cap \mathbf{C}^1(0, T, \mathbf{L}^2_\varepsilon(\Omega))\big) \times \big(\mathbf{C}(0, T, \mathbf{H}(\mathrm{div};\Omega)) \cap \mathbf{C}^1(0, T, \mathbf{L}^2_\mu(\Omega))\big)$ *of the system (1)–(2) satisfies*

$$\|\mathbf{E}\|_\varepsilon + \|\mathbf{H}\|_\mu \le \sqrt{2}\left[\|\mathbf{E}_0\|_\varepsilon + \|\mathbf{H}_0\|_\mu + \|\mathbf{J}\|_{\mathbf{L}^1\left(0,T,\mathbf{L}^2_{\varepsilon^{-1}}(\Omega)\right)}\right].$$

Proof: Take test functions $\Psi := \mathbf{E}$ and $\Phi := \mathbf{H}$ in (4)–(5) respectively, then

$$(\varepsilon \mathbf{E}_t, \mathbf{E}) - (\mathbf{H}, \nabla \times \mathbf{E}) = (\mathbf{J}, \mathbf{E}), \tag{6}$$

$$(\mu \mathbf{H}_t, \mathbf{H}) + (\nabla \times \mathbf{E}, \mathbf{H}) = 0. \tag{7}$$

Adding the equations (6)–(7), we have

$$(\varepsilon \mathbf{E}_t, \mathbf{E}) + (\mu \mathbf{H}_t, \mathbf{H}) = (\mathbf{J}, \mathbf{E}),$$

therefore

$$\frac{d}{dt}\left[\|\mathbf{E}\|_\varepsilon^2 + \|\mathbf{H}\|_\mu^2\right] = 2(\mathbf{J}, \mathbf{E}) \le 2\|\mathbf{J}\|_{\varepsilon^{-1}}\|\mathbf{E}\|_\varepsilon.$$

Integrating both sides from 0 to T, we obtain,

$$\begin{aligned}
&\|\mathbf{E}\|_\varepsilon^2 + \|\mathbf{H}\|_\mu^2\\
&\quad\le \|\mathbf{E}_0\|_\varepsilon^2 + \|\mathbf{H}_0\|_\mu^2 + 2\int_0^T \|\mathbf{J}\|_{\varepsilon^{-1}}\|\mathbf{E}\|_\varepsilon ds\\
&\quad\le \|\mathbf{E}_0\|_\varepsilon^2 + \|\mathbf{H}_0\|_\mu^2 + 2\int_0^T \|\mathbf{J}\|_{\varepsilon^{-1}}\sqrt{\|\mathbf{E}\|_\varepsilon^2 + \|\mathbf{H}\|_\mu^2}\, ds.
\end{aligned}$$

Then it follows from the Gronwall–Ou-Iang's inequality (see, e.g., [80]) that

$$\sqrt{\|\mathbf{E}\|_\varepsilon^2 + \|\mathbf{H}\|_\mu^2} \le \sqrt{\|\mathbf{E}_0\|_\varepsilon^2 + \|\mathbf{H}_0\|_\mu^2} + \int_0^T \|\mathbf{J}\|_{\varepsilon^{-1}} ds.$$

Since

$$\sqrt{\|\mathbf{E}\|_\varepsilon^2 + \|\mathbf{H}\|_\mu^2} \le \|\mathbf{E}\|_\varepsilon + \|\mathbf{H}\|_\mu \le \sqrt{2}\sqrt{\|\mathbf{E}\|_\varepsilon^2 + \|\mathbf{H}\|_\mu^2},$$

the statement follows. □

Let us now turn to time discretizations for the Maxwell system (1)–(2). The time interval $(0, T)$ is divided into $N \in \mathbb{N}$ equally spaced subintervals by using nodal points

$$0 =: t^0 < t^1 < t^2 < \cdots < t^N := T,$$

with $t^n = n\Delta t$, $\Delta t > 0$, $n = 0, 1, 2, \ldots, N$.

Replacing the time derivatives in (4)–(5) at t^n by the backward finite difference quotient, that is

$$\mathbf{E}_t(t^n) \approx \frac{\mathbf{E}(t^n) - \mathbf{E}(t^{n-1})}{\Delta t} \quad \text{etc.},$$

and get a sequence of problems of the type

$$\Big(\varepsilon \frac{\mathbf{E}^n - \mathbf{E}^{n-1}}{\Delta t}, \Psi\Big) - (\mathbf{H}^n, \nabla \times \Psi) = (\mathbf{J}^n, \Psi) \quad \forall\, \Psi \in \mathbf{H}_0(\mathrm{curl}; \Omega), \tag{8}$$

$$\Big(\mu \frac{\mathbf{H}^n - \mathbf{H}^{n-1}}{\Delta t}, \Phi\Big) + (\nabla \times \mathbf{E}^n, \Phi) = 0 \quad \forall\, \Phi \in \mathbf{H}(\mathrm{div}; \Omega), \tag{9}$$

where $(\mathbf{E}^n, \mathbf{H}^n) \in \mathbf{H}_0(\mathrm{curl}; \Omega) \times \mathbf{H}(\mathrm{div}; \Omega)$ are to be determined for $n \in \{1, \ldots, N\}$ (as approximations to $(\mathbf{E}(t^n), \mathbf{H}(t^n))$), $(\mathbf{E}^0, \mathbf{H}^0) \in \mathbf{H}_0(\mathrm{curl}; \Omega) \times \mathbf{H}(\mathrm{div}; \Omega)$ are given (as approximations to $(\mathbf{E}_0, \mathbf{H}_0)$), and $\mathbf{J}^n := \mathbf{J}(t^n) \in \mathbf{L}^2_{\varepsilon^{-1}}(\Omega)$.

Theorem 2: For $0 < \Delta t < 1/2$, there exists a constant $C > 0$ independent of Δt (but dependent on T) such that

$$\|\mathbf{E}^N\|_\varepsilon^2 + \|\mathbf{H}^N\|_\mu^2 \le C.$$

Proof: In (8)–(9), we choose the test functions $\Psi := 2\Delta t \mathbf{E}^n$ and $\Phi := 2\Delta t \mathbf{H}^n$. Then

$$2(\varepsilon(\mathbf{E}^n - \mathbf{E}^{n-1}), \mathbf{E}^n) - 2\Delta t(\mathbf{H}^n, \nabla \times \mathbf{E}^n) = 2\Delta t(\mathbf{J}^n, \mathbf{E}^n), \tag{10}$$

$$2(\mu(\mathbf{H}^n - \mathbf{H}^{n-1}), \mathbf{H}^n) + 2\Delta t(\nabla \times \mathbf{E}^n, \mathbf{H}^n) = 0. \tag{11}$$

Adding the equations (10) and (11), we get

$$2(\varepsilon(\mathbf{E}^n - \mathbf{E}^{n-1}), \mathbf{E}^n) + 2(\mu(\mathbf{H}^n - \mathbf{H}^{n-1}), \mathbf{H}^n) = 2\Delta t(\mathbf{J}^n, \mathbf{E}^n).$$

The identity (1) from Lemma 1 implies that

$$\|\mathbf{E}^n\|_\varepsilon^2 + \|\mathbf{E}^n - \mathbf{E}^{n-1}\|_\varepsilon^2 - \|\mathbf{E}^{n-1}\|_\varepsilon^2 + \|\mathbf{H}^n\|_\mu^2 + \|\mathbf{H}^n - \mathbf{H}^{n-1}\|_\mu^2 - \|\mathbf{H}^{n-1}\|_\mu^2 = 2\Delta t(\mathbf{J}^n, \mathbf{E}^n). \tag{12}$$

The right-hand side is estimated similarly to the proof of the inequality (2) from Lemma 1:

$$2(\mathbf{J}^n, \mathbf{E}^n) = 2(\varepsilon^{-1/2}\mathbf{J}^n, \varepsilon^{1/2}\mathbf{E}^n) \le \|\varepsilon^{-1/2}\mathbf{J}^n\|^2 + \|\varepsilon^{1/2}\mathbf{E}^n\|^2 = \|\mathbf{J}^n\|_{\varepsilon^{-1}}^2 + \|\mathbf{E}^n\|_\varepsilon^2.$$

Using this estimate in (12), we obtain

$$\|\mathbf{E}^n\|_\varepsilon^2 - \|\mathbf{E}^{n-1}\|_\varepsilon^2 + \|\mathbf{H}^n\|_\mu^2 - \|\mathbf{H}^{n-1}\|_\mu^2 \le \Delta t\|\mathbf{E}^n\|_\varepsilon^2 + \Delta t\|\mathbf{J}^n\|_{\varepsilon^{-1}}^2.$$

Summing up from $n = 1$ to N, we arrive at

$$\begin{aligned}\|\mathbf{E}^N\|_\varepsilon^2 + \|\mathbf{H}^N\|_\mu^2 &\le \Delta t \sum_{n=1}^N \|\mathbf{E}^n\|_\varepsilon^2 + \Delta t \sum_{n=1}^N \|\mathbf{J}^n\|_{\varepsilon^{-1}}^2 + \|\mathbf{E}^0\|_\varepsilon^2 + \|\mathbf{H}^0\|_\mu^2 \\ &\le \Delta t \sum_{n=0}^N \|\mathbf{E}^n\|_\varepsilon^2 + \Delta t \sum_{n=0}^N \|\mathbf{J}^n\|_{\varepsilon^{-1}}^2 + \|\mathbf{E}^0\|_\varepsilon^2 + \|\mathbf{H}^0\|_\mu^2.\end{aligned}$$

Now we are ready to apply Gronwall's inequality (Lemma 2) with $\delta := \Delta t \ge 0$, $g_0 := \|\mathbf{E}^0\|_\varepsilon^2 + \|\mathbf{H}^0\|_\mu^2 \ge 0$, $a_n := \|\mathbf{E}^n\|_\varepsilon^2 + \|\mathbf{H}^n\|_\mu^2 \ge 0$, $b_n := 0$, $c_n := \|\mathbf{J}^n\|_{\varepsilon^{-1}}^2 \ge 0$, and $\gamma_n := 1 \ge 0$. Then the condition $\gamma_n \delta < 1$ corresponds to $\Delta t < 1$ and the final estimate follows from the observation that $(n+1)\Delta t \le T + \Delta t \le T + 1/2$:

$$\begin{aligned}\|\mathbf{E}^N\|_\varepsilon^2 + \|\mathbf{H}^N\|_\mu^2 &\le \Big(\Delta t \sum_{n=0}^N \|\mathbf{J}^n\|_{\varepsilon^{-1}}^2 + \|\mathbf{E}^0\|_\varepsilon^2 + \|\mathbf{H}^0\|_\mu^2\Big) \times \exp\Big(\Delta t \sum_{n=0}^N (1 - \Delta t)^{-1}\Big) \\ &\le \Big(\sum_{n=0}^N \|\mathbf{J}^n\|_{\varepsilon^{-1}}^2 \Delta t + \|\mathbf{E}^0\|_\varepsilon^2 + \|\mathbf{H}^0\|_\mu^2\Big) \exp(2T + 1).\end{aligned}$$

It remains to note that the term $\sum_{n=0}^N \|\mathbf{J}^n\|_{\varepsilon^{-1}}^2 \Delta t$ is an approximation to $\int_0^T \|\mathbf{J}(t)\|_{\varepsilon^{-1}}^2 dt = \|\mathbf{J}\|^2_{\mathbf{L}^2(0,T,\mathbf{L}^2_{\varepsilon^{-1}}(\Omega))}$ and thus bounded. □

Next we want to prove an estimate of the error in time. To do so, we introduce the errors

$$\zeta_c^n := \mathbf{E}(t^n) - \mathbf{E}^n, \quad \xi_c^n := \mathbf{H}(t^n) - \mathbf{H}^n. \tag{13}$$

Theorem 3: If $(\mathbf{E}, \mathbf{H}) \in \big(\mathbf{C}(0, T, \mathbf{H}_0(\mathrm{curl}; \Omega)) \cap \mathbf{C}^2(0, T, \mathbf{L}^2_\varepsilon(\Omega))\big) \times \big(\mathbf{C}(0, T, \mathbf{H}(\mathrm{div}; \Omega)) \cap \mathbf{C}^2(0, T, \mathbf{L}^2_\mu(\Omega))\big)$ and if the time step Δt is sufficiently small, then there exists a constant $C > 0$ independent of Δt (but dependent on T) such that

$$\|\zeta_c^N\|_\varepsilon^2 + \|\xi_c^N\|_\mu^2 \le C\big(\Delta t + \|\zeta_c^0\|_\varepsilon + \|\xi_c^0\|_\mu\big).$$

Proof: From Taylor's formula with integral remainder it follows that

$$\mathbf{E}(t) = \mathbf{E}(t^n) + \mathbf{E}_t(t^n)(t - t^n) + \int_{t^n}^t (t - s)\mathbf{E}_{tt}(s) ds,$$

hence

$$\Big(\varepsilon \frac{\mathbf{E}(t^n) - \mathbf{E}(t^{n-1})}{\Delta t}, \Psi\Big) = (\varepsilon \mathbf{E}_t(t^n), \Psi) + (\varepsilon \mathbf{R}_{\mathbf{E}}^n, \Psi), \tag{14}$$

where

$$\mathbf{R}_{\mathbf{E}}^n := \frac{1}{\Delta t}\int_{t^{n-1}}^{t^n}(t^{n-1}-s)\mathbf{E}_{tt}(s)ds.$$

An analogous relation can be obtained with respect to $\mathbf{H}$. Making use of (4)–(5), we get

$$\Big(\varepsilon\frac{\mathbf{E}(t^n)-\mathbf{E}(t^{n-1})}{\Delta t},\Psi\Big)-(\mathbf{H}(t^n),\nabla\times\Psi) = (\mathbf{J}^n+\varepsilon\mathbf{R}_{\mathbf{E}}^n,\Psi)\quad\forall\,\Psi\in\mathbf{H}_0(\mathrm{curl};\Omega), \tag{15}$$

$$\Big(\mu\frac{\mathbf{H}(t^n)-\mathbf{H}(t^{n-1})}{\Delta t},\Phi\Big)+(\nabla\times\mathbf{E}(t^n),\Phi) = (\mu\mathbf{R}_{\mathbf{H}}^n,\Phi)\quad\forall\,\Phi\in\mathbf{H}(\mathrm{div};\Omega). \tag{16}$$

Now the equations (8)-(9) are subtracted from the equations (15)-(16). Together with (13) the result is:

$$\Big(\varepsilon\frac{\zeta_c^n-\zeta_c^{n-1}}{\Delta t},\Psi\Big)-\big(\xi_c^n,\nabla\times\Psi\big) = (\varepsilon\mathbf{R}_{\mathbf{E}}^n,\Psi) \tag{17}$$

$$\Big(\mu\frac{\xi_c^n-\xi_c^{n-1}}{\Delta t},\Phi\Big)+\big(\nabla\times\zeta_c^n,\Phi\big) = (\mu\mathbf{R}_{\mathbf{H}}^n,\Phi). \tag{18}$$

Taking $\Psi := 2\Delta t\zeta_c^n$ and $\Phi := 2\Delta t\xi_c^n$ in equations (17) and (18), by the same reasoning as in the proof of Theorem 2, from this we obtain the estimate

$$\|\zeta_c^n\|_\varepsilon^2-\|\zeta_c^{n-1}\|_\varepsilon^2+\|\xi_c^n\|_\mu^2-\|\xi_c^{n-1}\|_\mu^2 \le \Delta t\big[\|\zeta_c^n\|_\varepsilon^2+\|\xi_c^n\|_\mu^2\big]+\Delta t\Big[\|\mathbf{R}_{\mathbf{E}}^n\|_\varepsilon^2+\|\mathbf{R}_{\mathbf{H}}^n\|_\mu^2\Big].$$

The summation leads to

$$\begin{aligned}\|\zeta_c^N\|_\varepsilon^2+\|\xi_c^N\|_\mu^2 &\le \Big[\Delta t\sum_{n=1}^N\big[\|\zeta_c^n\|_\varepsilon^2+\|\xi_c^n\|_\mu^2\big]\\ &\quad+\Delta t\sum_{n=1}^N\Big[\|\mathbf{R}_{\mathbf{E}}^n\|_\varepsilon^2+\|\mathbf{R}_{\mathbf{H}}^n\|_\mu^2\Big]+\|\zeta_c^0\|_\varepsilon^2+\|\xi_c^0\|_\mu^2\Big].\end{aligned}$$

Next we apply Gronwall's inequality (Lemma 2) with $\delta := \Delta t \ge 0$, $g_0 := \|\zeta_c^0\|_\varepsilon^2+\|\xi_c^0\|_\mu^2 \ge 0$, $a_n := \|\zeta_c^n\|_\varepsilon^2+\|\xi_c^n\|_\mu^2 \ge 0$, $b_n := 0$, $c_n := \|\mathbf{R}_{\mathbf{E}}^n\|_\varepsilon^2+\|\mathbf{R}_{\mathbf{H}}^n\|_\mu^2 \ge 0$ $(n\ge 1)$, $c_0 := 0$, and $\gamma_n := 1 \ge 0$. Then the condition $\gamma_n\delta < 1$ corresponds to $\Delta t < 1$ and we get

$$\begin{aligned}\|\zeta_c^N\|_\varepsilon^2+\|\xi_c^N\|_\mu^2 &\le \Big[\Big(\Delta t\sum_{n=0}^N\Big[\|\mathbf{R}_{\mathbf{E}}^n\|_\varepsilon^2+\|\mathbf{R}_{\mathbf{H}}^n\|_\mu^2\Big]+\|\zeta_c^0\|_\varepsilon^2+\|\xi_c^0\|_\mu^2\Big)\\ &\quad\times\exp\Big(\Delta t\sum_{n=0}^N(1-\Delta t)^{-1}\Big)\Big]\\ &\le \Big[\Big(\sum_{n=0}^N\Big[\|\mathbf{R}_{\mathbf{E}}^n\|_\varepsilon^2+\|\mathbf{R}_{\mathbf{H}}^n\|_\mu^2\Big]\Delta t+\|\zeta_c^0\|_\varepsilon^2+\|\xi_c^0\|_\mu^2\Big)\\ &\quad\times\exp(2T+1)\Big].\end{aligned}$$

It remains to estimate the sum terms. Since

$$\begin{aligned}\|\mathbf{R}_{\mathbf{E}}^n\|_\varepsilon^2 &= \frac{1}{(\Delta t)^2}\left\|\int_{t^{n-1}}^{t^n}(t^{n-1}-s)\mathbf{E}_{tt}(s)ds.\right\|_\varepsilon^2\\ &\le \frac{1}{(\Delta t)^2}\int_{t^{n-1}}^{t^n}(s-t^{n-1})^2ds\int_{t^{n-1}}^{t^n}\|\mathbf{E}_{tt}(s)\|_\varepsilon^2ds\\ &= \frac{\Delta t}{3}\int_{t^{n-1}}^{t^n}\|\mathbf{E}_{tt}(s)\|_\varepsilon^2ds,\end{aligned}$$

it follows that

$$\begin{aligned}\sum_{n=0}^N\|\mathbf{R}_{\mathbf{E}}^n\|_\varepsilon^2\Delta t &\le \frac{(\Delta t)^2}{3}\int_0^T\|\mathbf{E}_{tt}(s)\|_\varepsilon^2ds\\ &= \frac{(\Delta t)^2}{3}\|\mathbf{E}_{tt}\|^2_{\mathbf{L}^2(0,T,\mathbf{L}^2_\varepsilon(\Omega))}.\end{aligned}$$

In summary, we get

$$\begin{aligned}&\|\zeta_c^N\|_\varepsilon^2+\|\xi_c^N\|_\mu^2\\ &\le\Big(\frac{(\Delta t)^2}{3}\Big[\|\mathbf{E}_{tt}\|^2_{\mathbf{L}^2(0,T,\mathbf{L}^2_\varepsilon(\Omega))}+\|\mathbf{H}_{tt}\|^2_{\mathbf{L}^2(0,T,\mathbf{L}^2_\mu(\Omega))}\Big]\\ &\quad+\|\zeta_c^0\|_\varepsilon^2+\|\xi_c^0\|_\mu^2\Big)\exp(2T+1).\end{aligned}$$

□

IV. SPATIAL DISCRETIZATION

In this section we introduce families of finite dimensional subspaces $\mathbf{U}_h\subset\mathbf{H}(\mathrm{curl};\Omega)$ and $\mathbf{V}_h\subset\mathbf{H}(\mathrm{div};\Omega)$ to discretize the problem (8)–(9) in space.

Let $\mathcal{T}_h$ be an arbitrary member of a family of triangulations of Ω consisting of geometric elements K. Each element $K\in\mathcal{T}_h$ is assumed to be an open tetrahedron if K has no face or edge on Γ. The elements that have an edge or face on Γ are allowed to have one curved edge or one curved face, respectively. These elements are called boundary elements [16]. If K is a boundary element we assign a standard tetrahedron $\tilde{K}$ by connecting the four vertices of K by straight edges.

In addition, all triangulations should be compatible with the discontinuities of the coefficients ε and μ, that is their discontinuities lie on the boundaries of the elements of the triangulations only. Moreover we assume that the family of triangulations is quasi-uniform. That is, there exist constants $\underline{c}_{\mathcal{F}}>0$, $\overline{c}_{\mathcal{F}}>0$ independent of K and $\mathcal{T}_h$ such that

$$\underline{c}_{\mathcal{F}}h\le h_K\le\overline{c}_{\mathcal{F}}\rho_K\quad\forall K\in\mathcal{T}_h\,\forall\mathcal{T}_h,$$

where ρ_K is the maximum diameter of the largest ball contained in K or $\tilde{K}$, h_K is the diameter of K and $h := \max_{K\in\mathcal{T}_h}h_K$ [78].

Now let Ω_h be the interior of the set

$$\bigcup_{K\in\mathcal{T}_h}\overline{\tilde{K}}.$$

Let $\mathcal{P}_k$ be the space of scalar real-valued polynomials in three variables of maximal degree k, and $\tilde{\mathcal{P}}_k$ be the space of scalar real-valued homogeneous polynomials of exact degree k.

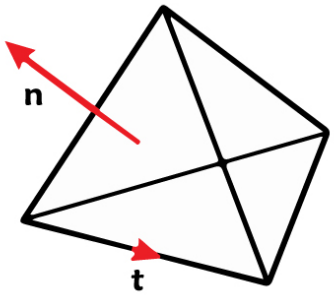

FIGURE 1. A tetrahedron K: $\mathbf{t}$ is an edge tangent vector, $\mathbf{n}$ is a face normal.

For any $k \in \mathbb{N}$, we define the following subspaces of $\mathbf{P}_k := [\mathcal{P}_k]^3$ (for details see [65]), [71] or [72]:

$$\begin{aligned}\mathbf{D}_k &:= \mathbf{P}_{k-1} \oplus \mathbf{x}\,\tilde{\mathcal{P}}_{k-1},\\ \mathbf{S}_k &:= \{\mathbf{p} \in [\tilde{\mathcal{P}}_k]^3 :\ \mathbf{x}\cdot\mathbf{p}(\mathbf{x}) = 0\},\\ \mathbf{R}_k &:= \mathbf{P}_{k-1} \oplus \mathbf{S}_k.\end{aligned}$$

Obviously, $\mathbf{S}_k \subset \mathbf{P}_k$ and $\mathbf{R}_k \subset \mathbf{P}_k$.

Here we describe the so-called first family of Nédélec edge elements. We mention that in the two definitions below it is assumed that a standard reference tetrahedron $\hat{K}$ is used and that an affine transformation between $\hat{K}$ and K is applied.

Definition 1 ($\mathbf{R}_k$-Unisolvent and Curl-Conforming Dofs): Let K be a tetrahedron in $\mathbb{R}^3$ with faces denoted by f and edges denoted by e. $\mathbf{t}$ and $\mathbf{n}$ in Fig (1) represent the unit vectors along the edge e and perpendicular to the face f, respectively. Let $\mathbf{v} \in \mathbf{W}^{1,p}(K)$ for some $p > 2$. We define the following three sets of moments of $\mathbf{v}$ on K:

$$\begin{aligned}&\text{For the six edges of } e \text{ of } K\\ M_e(\mathbf{v}) &:= \left\{\int_e \mathbf{v}\cdot\mathbf{t}\,q\,de \quad \forall q \in P_{k-1}(e)\right\},\\ &\text{for the four faces} f \text{ of } K\\ M_f(\mathbf{v}) &:= \left\{\int_f \mathbf{v}\times\mathbf{n}\cdot\mathbf{q}\,ds \quad \forall \mathbf{q} \in [P_{k-2}(f)]^2\right\},\\ M_K(\mathbf{v}) &:= \left\{\int_K \mathbf{v}\cdot\mathbf{q}\,d\mathbf{x} \quad \forall \mathbf{q} \in \mathbf{P}_{k-3}(K)\right\}.\end{aligned}$$

Remark 1: The dofs M_f are given here in the original version of [71], Def. 4. However, from the point of view of affine equivalence it may be useful to use a different, but equivalent representation [65], Remark 5.31.

This set of moments is $\mathbf{R}_k$-unisolvent and curl-conforming as proved in [71], Thm. 1. For any $\mathbf{v} \in \mathbf{W}^{1,p}(K)$, we define a local interpolant $\mathbf{r}_K\mathbf{v} \in \mathbf{R}_k$ such that

$$M_e(\mathbf{v} - \mathbf{r}_K\mathbf{v}) = M_f(\mathbf{v} - \mathbf{r}_K\mathbf{v}) = M_K(\mathbf{v} - \mathbf{r}_K\mathbf{v}) = \{0\}$$

The global interpolant $\mathbf{r}_h\mathbf{v} \in \mathbf{U}_h := \{\mathbf{w} \in \mathbf{H}(\mathrm{curl};\Omega) : \mathbf{w}|_K \in \mathbf{R}_k\ \forall K \in \mathcal{T}_h\}$ is defined element-wise:

$$\mathbf{r}_h\mathbf{v}|_K := \mathbf{r}_K(\mathbf{v}|_K) \quad \forall K \in \mathcal{T}_h.$$

The following estimate holds for $\mathbf{r}_h$ ([71], Thm. 2): If $\mathbf{v} \in \mathbf{H}^{k+1}(\Omega)$ then

$$\|\mathbf{v} - \mathbf{r}_h\mathbf{v}\|_{\mathbf{H}(\mathrm{curl};\Omega)} \le Ch^k\|\mathbf{v}\|_{\mathbf{H}^{k+1}(\Omega)}.$$

Definition 2 ($\mathbf{D}_k$-Unisolvent and Div-Conforming Dofs): Let K be a tetrahedron in $\mathbb{R}^3$ with faces denoted by f with normal $\mathbf{n}$. Let $\mathbf{v} \in \mathbf{W}^{1,p}(K)$ for some $p > 2$. We define the following two set of moments of $\mathbf{v}$ on K:

$$\begin{aligned}&\text{For the four faces} f \text{ of } K\\ M_f(\mathbf{v}) &:= \left\{\int_f \mathbf{v}\cdot\mathbf{n}\,q,ds \quad \forall q \in P_{k-1}(f)\right\},\\ M_K(\mathbf{v}) &:= \left\{\int_K \mathbf{v}\cdot\mathbf{q}\,d\mathbf{x} \quad \forall \mathbf{q} \in \mathbf{P}_{k-2}(K)\right\}.\end{aligned}$$

This set of moments is $\mathbf{D}_k$-unisolvent and div-conforming as proved in [71], Thm. 3. For any $\mathbf{v} \in \mathbf{W}^{1,p}(K)$, we define a local interpolant $\mathbf{w}_K\mathbf{v} \in \mathbf{D}_k$ as follows:

$$M_f(\mathbf{v} - \mathbf{w}_K\mathbf{v}) = M_K(\mathbf{v} - \mathbf{w}_K\mathbf{v}) = \{0\}.$$

The global interpolant $\mathbf{w}_h\mathbf{v} \in \mathbf{V}_h := \{\mathbf{w} \in \mathbf{H}(\mathrm{div};\Omega) : \mathbf{w}|_K \in \mathbf{D}_k\ \forall K \in \mathcal{T}_h\}$ is defined element-wise:

$$\mathbf{w}_h\mathbf{v}|_K := \mathbf{w}_K(\mathbf{v}|_K) \quad \forall K \in \mathcal{T}_h.$$

An error estimate also holds for $\mathbf{w}_h$ (see [18], equation (19), and [71], Thm. 4): If $\mathbf{v} \in \mathbf{H}^k(\Omega)$, then

$$\|\mathbf{v} - \mathbf{w}_h\mathbf{v}\|_\varepsilon \le Ch^k\|\mathbf{v}\|_{\mathbf{H}^k(\Omega)}.$$

According to [65], Lemma 5.40, the spaces $\mathbf{U}_h$ and $\mathbf{V}_h$ are related via

$$\nabla\times\mathbf{U}_h \subset \mathbf{V}_h, \tag{19}$$

and the interpolation operators $\mathbf{r}_h$ and $\mathbf{w}_h$ are linked together as follows: $\nabla\times\mathbf{r}_h\mathbf{v} = \mathbf{w}_h(\nabla\times\mathbf{v})$ for all $\mathbf{v}$ such that both the interpolants $\mathbf{r}_h\mathbf{v}$ and $\mathbf{w}_h(\nabla\times\mathbf{v})$ are defined.

In the subsequent error analysis, we will make use of two projection operators into $\mathbf{U}_{0h} := \mathbf{U}_h \cap \mathbf{H}_0(\mathrm{curl};\Omega)$ and $\mathbf{V}_h$, respectively. The first projection operator $\Pi_h : \mathbf{H}_0(\mathrm{curl};\Omega) \to \mathbf{U}_{0h}$ is defined by

$$\begin{aligned}\left(\nabla\times\Pi_h\mathbf{u}, \Psi_h\right) &= \left(\nabla\times\mathbf{u}, \Psi_h\right) \quad \forall\Psi_h \in \mathbf{V}_h,\\ (\Pi_h\mathbf{u}, \nabla p_h) &= (\mathbf{u}, \nabla p_h) \quad \forall p_h \in S_h^k,\end{aligned} \tag{20}$$

where S_h^k is the standard space of continuous finite elements on $\mathcal{T}_h$:

$$S_h^k := \{v \in H_0^1(\Omega) :\ v|_K \in \mathcal{P}_k\ \forall K \in \mathcal{T}_h\},$$

see [17].

An error bound for the projection Π_h can be derived as in [18]: If $\mathbf{u} \in \mathbf{H}^{k+1}(\Omega)$, then

$$\|\mathbf{u} - \Pi_h\mathbf{u}\|_\varepsilon \le Ch^k\|\mathbf{u}\|_{\mathbf{H}^{k+1}(\Omega)}. \tag{21}$$

The second projection operator is the $\mathbf{L}^2$-orthogonal projection of $\mathbf{H}(\mathrm{div};\Omega)$ onto $\mathbf{V}_h$:

$$(\mathbf{P}_h\mathbf{H}, \Phi_h) = (\mathbf{H}, \Phi_h) \quad \forall\Phi_h \in \mathbf{V}_h. \tag{22}$$

By the help of similar arguments as in [18], the following estimate can be shown for $\mathbf{v} \in \mathbf{H}^k(\Omega)$:

$$\|\mathbf{P}_h\mathbf{v} - \mathbf{v}\|_\mu \le Ch^k\|\mathbf{u}\|_{\mathbf{H}^k(\Omega)}. \tag{23}$$

V. FULL DISCRETIZATION USING THE BACKWARD EULER METHOD

The fully discrete electric and magnetic fields $(\mathbf{E}_h^n, \mathbf{H}_h^n) \in \mathbf{U}_{0h} \times \mathbf{V}_h$ satisfy

$$\Big(\varepsilon \frac{\mathbf{E}_h^n - \mathbf{E}_h^{n-1}}{\Delta t}, \Psi_h\Big) - (\mathbf{H}_h^n, \nabla \times \Psi_h) = (\mathbf{J}^n, \Psi_h) \quad \forall\, \Psi_h \in \mathbf{U}_{0h}, \tag{24}$$

$$\Big(\mu \frac{\mathbf{H}_h^n - \mathbf{H}_h^{n-1}}{\Delta t}, \Phi_h\Big) + (\nabla \times \mathbf{E}_h^n, \Phi_h) = 0 \quad \forall\, \Phi_h \in \mathbf{V}_h, \tag{25}$$

where $(\mathbf{E}_h^n, \mathbf{H}_h^n) \in \mathbf{U}_{0h} \times \mathbf{V}_h$ are to be determined for $n \in \{1, \ldots, N\}$ and $(\mathbf{E}_h^0, \mathbf{H}_h^0) \in \mathbf{U}_{0h} \times \mathbf{V}_h$ are given (and will be specified later). Before formulating the theorem, we still introduce a few terms. The full error of the electric field will be denoted by

$$\zeta^n := \mathbf{E}(t^n) - \mathbf{E}_h^n = \eta^n - \eta_h^n, \tag{26}$$

where

$$\eta^n := \mathbf{E}(t^n) - \Pi_h \mathbf{E}(t^n), \quad \eta_h^n := \mathbf{E}_h^n - \Pi_h \mathbf{E}(t^n). \tag{27}$$

Similarly for the magnetic field:

$$\xi^n := \mathbf{H}(t^n) - \mathbf{H}_h^n = \theta^n - \theta_h^n \tag{28}$$

with

$$\theta^n := \mathbf{H}(t^n) - \mathbf{P}_h \mathbf{H}(t^n), \quad \theta_h^n := \mathbf{H}_h^n - \mathbf{P}_h \mathbf{H}(t^n). \tag{29}$$

Theorem 4: Let $(\mathbf{E}, \mathbf{H})$ *be the solution of (4)–(5) such that, for some* $k \in \mathbb{N}$,

$$\mathbf{E} \in C(0, T, \mathbf{H}_0(\mathrm{curl};\, \Omega)) \cap C^2(0, T, \mathbf{L}_\varepsilon^2(\Omega) \cap \mathbf{H}^{k+1}(\Omega)),$$
$$\mathbf{H} \in C^2(0, T, \mathbf{L}_\mu^2(\Omega) \cap \mathbf{H}^k(\Omega)),$$

and $(\mathbf{E}_h^n, \mathbf{H}_h^n)$ *be the fully discrete solution of (24)-(25). Then, for sufficiently small* Δt *and* h*, the following error estimate holds:*

$$\|\zeta^N\|_\varepsilon + \|\xi^N\|_\mu \le C\big[\Delta t + h^k + h^k \Delta t\big],$$

where the constant $C > 0$ *does not depend on* Δt *and* h *(the structure of* C *will be seen from the proof).*

Proof: Taking $\Psi = \Psi_h$ and $\Phi = \Phi_h$ in (15)-(16), subtracting the system (24)-(25) from the system (4)–(5) and using the definitions (26), (28), we obtain:

$$\Big(\varepsilon \frac{\zeta^n - \zeta^{n-1}}{\Delta t}, \Psi_h\Big) - (\xi^n, \nabla \times \Psi_h) = (\varepsilon \mathbf{R}_\mathbf{E}^n, \Psi_h),$$
$$\Big(\mu \frac{\xi^n - \xi^{n-1}}{\Delta t}, \Phi_h\Big) + (\nabla \times \zeta^n, \Phi_h) = (\mu \mathbf{R}_\mathbf{H}^n, \Phi_h).$$

Furthermore, using the decompositions (27), (29), after a simple rearrangement we arrive at

$$\Big(\varepsilon \frac{(\eta^n - \eta^{n-1}) - (\eta_h^n - \eta_h^{n-1})}{\Delta t}, \Psi_h\Big) - (\theta^n - \theta_h^n, \nabla \times \Psi_h) = (\varepsilon \mathbf{R}_\mathbf{E}^n, \Psi_h),$$

$$\Big(\mu \frac{(\theta^n - \theta^{n-1}) - (\theta_h^n - \theta_h^{n-1})}{\Delta t}, \Phi_h\Big) + (\nabla \times (\eta^n - \eta_h^n), \Phi_h) = (\mu \mathbf{R}_\mathbf{H}^n, \Phi_h).$$

Now we set $\Psi_h := -2\Delta t \eta_h^n$ and $\Phi_h := -2\Delta t \theta_h^n$:

$$\begin{aligned}
2\big(\varepsilon(\eta_h^n - \eta_h^{n-1}), \eta_h^n\big) - 2\Delta t(\theta_h^n, \nabla \times \eta_h^n) &= 2\big(\varepsilon(\eta^n - \eta^{n-1}), \eta_h^n\big) \\
&\quad - 2\Delta t(\theta^n, \nabla \times \eta_h^n) - 2\Delta t(\varepsilon \mathbf{R}_\mathbf{E}^n, \eta_h^n) \\
2\big(\mu(\theta_h^n - \theta_h^{n-1}), \theta_h^n\big) + 2\Delta t\big(\nabla \times \eta_h^n, \theta_h^n\big) &= 2\big(\mu(\theta^n - \theta^{n-1}), \theta_h^n\big) \\
&\quad + 2\Delta t\big(\nabla \times \eta^n, \theta_h^n\big) - 2\Delta t(\mu \mathbf{R}_\mathbf{H}^n, \theta_h^n).
\end{aligned}$$

Thanks to (20), (22) and (19), the middle terms on the right-hand sides vanish. Adding the resulting equations, we get

$$\begin{aligned}
2\big(\varepsilon(\eta_h^n - \eta_h^{n-1}), \eta_h^n\big) + 2\big(\mu(\theta_h^n - \theta_h^{n-1}), \theta_h^n\big) &= 2\big(\varepsilon(\eta^n - \eta^{n-1}), \eta_h^n\big) + 2\big(\mu(\theta^n - \theta^{n-1}), \theta_h^n\big) \\
&\quad - 2\Delta t(\varepsilon \mathbf{R}_\mathbf{E}^n, \eta_h^n) - 2\Delta t(\mu \mathbf{R}_\mathbf{H}^n, \theta_h^n).
\end{aligned}$$

Now the identity (1) from Lemma 1 allows to rewrite the left-hand side as,

$$\begin{aligned}
&\|\eta_h^n\|_\varepsilon^2 + \|\eta_h^n - \eta_h^{n-1}\|_\varepsilon^2 - \|\eta_h^{n-1}\|_\varepsilon^2 + \|\theta_h^n\|_\mu^2 \\
&\qquad + \|\theta_h^n - \theta_h^{n-1}\|_\mu^2 - \|\theta_h^{n-1}\|_\mu^2 \\
&\quad = 2\big(\varepsilon(\eta^n - \eta^{n-1}), \eta_h^n\big) + 2\big(\mu(\theta^n - \theta^{n-1}), \theta_h^n\big) \\
&\qquad - 2\Delta t(\varepsilon \mathbf{R}_\mathbf{E}^n, \eta_h^n) - 2\Delta t(\mu \mathbf{R}_\mathbf{H}^n, \theta_h^n).
\end{aligned} \tag{30}$$

The first two terms on the right-hand side are treated by means of formula (14). Namely, replacing there $\mathbf{E}(t^n)$ by $(\mathbf{I} - \Pi_h)\mathbf{E}(t^n)$, we obtain

$$\begin{aligned}
\big(\varepsilon(\eta^n - \eta^{n-1}), \eta_h^n\big) &= \Delta t(\varepsilon(\mathbf{I} - \Pi_h)\mathbf{E}_t(t^n), \eta_h^n) \\
&\quad + \Delta t(\varepsilon(\mathbf{I} - \Pi_h)\mathbf{R}_\mathbf{E}^n, \eta_h^n).
\end{aligned}$$

In the same way we get

$$\begin{aligned}
\big(\mu(\theta^n - \theta^{n-1}), \theta_h^n\big) &= \Delta t(\mu(\mathbf{I} - \mathbf{P}_h)\mathbf{H}_t(t^n), \theta_h^n) \\
&\quad + \Delta t(\mu(\mathbf{I} - \mathbf{P}_h)\mathbf{R}_\mathbf{H}^n, \theta_h^n).
\end{aligned}$$

Using this in (30) and applying the estimate (2) from Lemma 1 to each of the resulting terms on the right-hand side, we obtain

$$\begin{aligned}
&\|\eta_h^n\|_\varepsilon^2 + \|\eta_h^n - \eta_h^{n-1}\|_\varepsilon^2 - \|\eta_h^{n-1}\|_\varepsilon^2 + \|\theta_h^n\|_\mu^2 \\
&\quad + \|\theta_h^n - \theta_h^{n-1}\|_\mu^2 - \|\theta_h^{n-1}\|_\mu^2 \\
&\le \Delta t\|(\mathbf{I} - \Pi_h)\mathbf{E}_t(t^n)\|_\varepsilon^2 + \Delta t\|(\mathbf{I} - \Pi_h)\mathbf{R}_\mathbf{E}^n\|_\varepsilon^2 + \Delta t\|\mathbf{R}_\mathbf{E}^n\|_\varepsilon^2 \\
&\quad + 3\Delta t\|\eta_h^n\|_\varepsilon^2 + \Delta t\|(\mathbf{I} - \mathbf{P}_h)\mathbf{H}_t(t^n)\|_\mu^2 + \Delta t\|(\mathbf{I} - \mathbf{P}_h)\mathbf{R}_\mathbf{H}^n\|_\mu^2 \\
&\quad + \Delta t\|\mathbf{R}_\mathbf{H}^n\|_\mu^2 + 3\Delta t\|\theta_h^n\|_\mu^2
\end{aligned}$$

Summing up from $n = 1$ to N and ignoring the second and fifth terms on the left-hand side, we arrive at

$$\begin{aligned}
\|\eta_h^N\|_\varepsilon^2 + \|\theta_h^N\|_\mu^2 &\le 3\Delta t \sum_{n=1}^N \big[\|\eta_h^n\|_\varepsilon^2 + \|\theta_h^n\|_\mu^2\big] \\
&\quad + \Delta t \sum_{n=1}^N \Big[\|(\mathbf{I} - \Pi_h)\mathbf{E}_t(t^n)\|_\varepsilon^2 + \|(\mathbf{I} - \Pi_h)\mathbf{R}_\mathbf{E}^n\|_\varepsilon^2 + \|\mathbf{R}_\mathbf{E}^n\|_\varepsilon^2 \\
&\quad + \|(\mathbf{I} - \mathbf{P}_h)\mathbf{H}_t(t^n)\|_\mu^2 + \|(\mathbf{I} - \mathbf{P}_h)\mathbf{R}_\mathbf{H}^n\|_\mu^2 + \|\mathbf{R}_\mathbf{H}^n\|_\mu^2\Big] \\
&\quad + \|\eta_h^0\|_\varepsilon^2 + \|\theta_h^0\|_\mu^2.
\end{aligned}$$

Now we are ready to apply Gronwall's inequality (Lemma 2) with $\delta := \Delta t \ge 0$, $g_0 := \|\eta_h^0\|_\varepsilon^2 + \|\theta_h^0\|_\mu^2 \ge 0$,

$a_n := \|\eta_h^n\|_\varepsilon^2 + \|\theta_h^n\|_\mu^2 \geq 0, b_n := 0, c_n := \|(\mathbf{I}-\Pi_h)\mathbf{E}_t(t^n)\|_\varepsilon^2 + \|(\mathbf{I}-\Pi_h)\mathbf{R}_\mathbf{E}^n\|_\varepsilon^2 + \|\mathbf{R}_\mathbf{E}^n\|_\varepsilon^2 + \|(\mathbf{I}-\mathbf{P}_h)\mathbf{H}_t(t^n)\|_\mu^2 + \|(\mathbf{I}-\mathbf{P}_h)\mathbf{R}_\mathbf{H}^n\|_\mu^2 + \|\mathbf{R}_\mathbf{H}^n\|_\mu^2 \geq 0$, and $\gamma_n := 3 \geq 0$. Then the condition $\gamma_n \delta < 1$ corresponds to $\Delta t < 1/3$ and we obtain, say for $\Delta t < 1/6$,

$$\begin{aligned}
&\|\eta_h^N\|_\varepsilon^2 + \|\theta_h^N\|_\mu^2 \\
&\quad \leq \Bigg(\Delta t \sum_{n=0}^{N} \Big[\|(\mathbf{I}-\Pi_h)\mathbf{E}_t(t^n)\|_\varepsilon^2 + \|(\mathbf{I}-\Pi_h)\mathbf{R}_\mathbf{E}^n\|_\varepsilon^2 \\
&\qquad + \|\mathbf{R}_\mathbf{E}^n\|_\varepsilon^2 + \|(\mathbf{I}-\mathbf{P}_h)\mathbf{H}_t(t^n)\|_\mu^2 + \|(\mathbf{I}-\mathbf{P}_h)\mathbf{R}_\mathbf{H}^n\|_\mu^2 \\
&\qquad + \|\mathbf{R}_\mathbf{H}^n\|_\mu^2 \Big] + \|\eta_h^0\|_\varepsilon^2 + \|\theta_h^0\|_\mu^2 \Bigg) \exp(6T+1).
\end{aligned}$$

From the end of the proof of Thm. 3 it is known that

$$\begin{aligned}
&\Delta t \sum_{n=0}^{N} \big[\|\mathbf{R}_\mathbf{E}^n\|_\varepsilon^2 + \|\mathbf{R}_\mathbf{H}^n\|_\mu^2 \big] \\
&\qquad \leq \frac{(\Delta t)^2}{3} \big[\|\mathbf{E}_{tt}\|^2_{\mathbf{L}^2(0,T,\mathbf{L}^2_\varepsilon(\Omega))} + \|\mathbf{H}_{tt}\|^2_{\mathbf{L}^2(0,T,\mathbf{L}^2_\mu(\Omega))} \big].
\end{aligned}$$

Furthermore, from (21) we see that,

$$\begin{aligned}
\|(\mathbf{I}-\Pi_h)\mathbf{E}_t(t^n)\|_\varepsilon &\leq Ch^k \|\mathbf{E}_t(t^n)\|_{\mathbf{H}^{k+1}(\Omega)}, \\
\|(\mathbf{I}-\Pi_h)\mathbf{R}_\mathbf{E}^n\|_\varepsilon &\leq Ch^k \|\mathbf{R}_\mathbf{E}^n\|_{\mathbf{H}^{k+1}(\Omega)},
\end{aligned}$$

and (23) yields the estimates,

$$\begin{aligned}
\|(\mathbf{I}-\mathbf{P}_h)\mathbf{H}_t(t^n)\|_\mu &\leq Ch^k \|\mathbf{H}_t(t^n)\|_{\mathbf{H}^k(\Omega)} \\
\|(\mathbf{I}-\mathbf{P}_h)\mathbf{R}_\mathbf{H}^n\|_\mu &\leq Ch^k \|\mathbf{R}_\mathbf{H}^n\|_{\mathbf{H}^k(\Omega)}.
\end{aligned}$$

Therefore,

$$\begin{aligned}
&\Delta t \sum_{n=0}^{N} \big[\|(\mathbf{I}-\Pi_h)\mathbf{E}_t(t^n)\|_\varepsilon^2 + \|(\mathbf{I}-\mathbf{P}_h)\mathbf{H}_t(t^n)\|_\mu^2 \big] \\
&\quad \leq Ch^{2k} \sum_{n=0}^{N} \big[\|\mathbf{E}_t(t^n)\|^2_{\mathbf{H}^{k+1}(\Omega)} + \|\mathbf{H}_t(t^n)\|^2_{\mathbf{H}^k(\Omega)} \big] \Delta t \\
&\quad \leq Ch^{2k} \int_0^T \big[\|\mathbf{E}_t(t)\|^2_{\mathbf{H}^{k+1}(\Omega)} + \|\mathbf{H}_t(t)\|^2_{\mathbf{H}^k(\Omega)} \big] dt \\
&\quad = Ch^{2k} \big[\|\mathbf{E}_t\|^2_{\mathbf{L}^2(0,T,\mathbf{H}^{k+1}(\Omega))} + \|\mathbf{H}_t\|^2_{\mathbf{L}^2(0,T,\mathbf{H}^k(\Omega))} \big],
\end{aligned}$$

and

$$\begin{aligned}
&\Delta t \sum_{n=0}^{N} \big[\|(\mathbf{I}-\Pi_h)\mathbf{R}_\mathbf{E}^n\|_\varepsilon^2 + \|(\mathbf{I}-\mathbf{P}_h)\mathbf{R}_\mathbf{H}^n\|_\mu^2 \big] \\
&\quad \leq Ch^{2k} \sum_{n=0}^{N} \big[\|\mathbf{R}_\mathbf{E}^n\|^2_{\mathbf{H}^{k+1}(\Omega)} + \|\mathbf{R}_\mathbf{H}^n\|^2_{\mathbf{H}^k(\Omega)} \big] \Delta t \\
&\quad \leq Ch^{2k} (\Delta t)^2 \big[\|\mathbf{E}_{tt}\|^2_{\mathbf{L}^2(0,T,\mathbf{H}^{k+1}(\Omega))} + \|\mathbf{H}_{tt}\|^2_{\mathbf{L}^2(0,T,\mathbf{H}^k(\Omega))} \big].
\end{aligned}$$

Finally, if we take

$$\mathbf{E}_h^0 := \Pi_h \mathbf{E}_0, \quad \mathbf{H}_h^0 := \mathbf{P}_h \mathbf{H}_0, \tag{31}$$

we conclude that,

$$\|\eta_h^N\|_\varepsilon + \|\theta_h^N\|_\mu \leq C\big[\Delta t + h^k + h^k \Delta t\big].$$

The terms $\|\eta^N\|_\varepsilon$ and $\|\theta^N\|_\mu$ are estimated by (21) and (23), respectively:

$$\begin{aligned}
\|\eta^N\|_\varepsilon &= \|(\mathbf{I}-\Pi_h)\mathbf{E}(t^N)\|_\varepsilon \leq Ch^k \|\mathbf{E}(t^N)\|_{\mathbf{H}^{k+1}(\Omega)}, \\
\|\theta^N\|_\mu &= \|(\mathbf{I}-\mathbf{P}_h)\mathbf{H}(t^N)\|_\mu \leq Ch^k \|\mathbf{H}(t^N)\|_{\mathbf{H}^k(\Omega)}.
\end{aligned}$$

The triangle inequality yields the stated result:

$$\begin{aligned}
&\|\mathbf{E}(t^N) - \mathbf{E}_h^N\|_\varepsilon + \|\mathbf{H}(t^N) - \mathbf{H}_h^N\|_\mu \\
&\quad \leq \|\eta^N\|_\varepsilon + \|\eta_h^N\|_\varepsilon + \|\theta^N\|_\mu + \|\theta_h^N\|_\mu \\
&\quad \leq C\big[\Delta t + h^k + h^k \Delta t\big].
\end{aligned}$$

□

VI. NUMERICAL RESULTS

Denoting by $\mathbf{e}^n$, $\mathbf{h}^n$ and $\mathbf{j}^n$ the representation vectors of $\mathbf{E}_h^n$, $\mathbf{H}_h^n$ and the $\mathbf{L}^2$-orthogonal projection of $\mathbf{J}^n$ onto $\mathbf{U}_{0h}$, the method (24)–(25) can be written as follows:

$$\mathbf{M}_\varepsilon \frac{\mathbf{e}^n - \mathbf{e}^{n-1}}{\Delta t} = \mathbf{G}^\top \mathbf{h}^n + \mathbf{j}^n, \tag{32}$$

$$\mathbf{M}_\mu \frac{\mathbf{h}^n - \mathbf{h}^{n-1}}{\Delta t} = -\mathbf{G}\mathbf{e}^n, \tag{33}$$

where $\mathbf{M}_\varepsilon$ is the positively definite mass matrix of size $\dim \mathbf{U}_{0h} \times \dim \mathbf{U}_{0h}$ for the material parameter ε, $\mathbf{M}_\mu$ is the positively definite mass matrix of size $\dim \mathbf{V}_h \times \dim \mathbf{V}_h$ for the material parameter μ, and $\mathbf{G}$ is a discrete representation of $-\mathrm{curl}$ with size $\dim \mathbf{V}_h \times \dim \mathbf{U}_{0h}$.

A. IMPLEMENTATION OF THE BACKWARD EULER METHOD

The formal algorithm for the system (32)-(33) reads as follows:

Compute the number of time steps:

$$nstep := \frac{T - t_0}{\Delta t}$$

Compute the initial values for the electric and magnetic fields:

$\mathbf{e}^0 \leftarrow \mathbf{E}_0$

$\mathbf{h}^0 \leftarrow \mathbf{H}_0$

Loop over time steps:

`for` $n = 1$ `to` *nstep* `do:`

Begin integration method update:

$\mathbf{e}_{in} \leftarrow \mathbf{e}^{n-1}$

$\mathbf{h}_{in} \leftarrow \mathbf{h}^{n-1}$

Update the electric and magnetic fields values:

$\mathbf{e}_{out} \leftarrow \mathbf{e}_{in} + \Delta t \mathbf{M}_\varepsilon^{-1} \big(\mathbf{G}^\top \mathbf{h}_{out} + \mathbf{j}^n \big)$

$\mathbf{h}_{out} \leftarrow \mathbf{h}_{in} + \Delta t \mathbf{M}_\mu^{-1} \mathbf{G} \mathbf{e}_{out}$

Update the electric and magnetic fields values for this time step:

$\mathbf{e}^n \leftarrow \mathbf{e}_{out}$

$\mathbf{h}^n \leftarrow \mathbf{h}_{out}$

`end for`

Completion:

$\mathbf{e}^N \leftarrow \mathbf{e}^{nstep}$

$\mathbf{h}^N \leftarrow \mathbf{h}^{nstep}$

B. IMPLEMENTATION OF THE SYMPLECTIC METHOD

We have also tested the application of symplectic time integration methods. A 4th order symplectic integration algorithm for the time dependent Maxwell's equations with parameters

$$\beta_1 = \frac{2+2^{\frac{1}{3}}+2^{-\frac{1}{3}}}{6}, \quad \alpha_1 = 0,$$
$$\beta_2 = \frac{1-2^{\frac{1}{3}}-2^{-\frac{1}{3}}}{6}, \quad \alpha_2 = \frac{1}{2-2^{\frac{1}{3}}},$$
$$\beta_3 = \frac{1-2^{\frac{1}{3}}-2^{-\frac{1}{3}}}{6}, \quad \alpha_3 = \frac{1}{1-2^{\frac{2}{3}}},$$
$$\beta_4 = \frac{2+2^{\frac{1}{3}}+2^{-\frac{1}{3}}}{6}, \quad \alpha_4 = \frac{1}{2-2^{\frac{1}{3}}}$$

(see [81], [82]) is given as follows:

Compute the number of time steps:

$$nstep := \frac{T-t_0}{\Delta t}$$

Compute the initial values for the electric and magnetic fields:

$\mathbf{e}^0 \leftarrow \mathbf{E}_0$

$\mathbf{h}^0 \leftarrow \mathbf{H}_0$

Loop over time steps:

`for` $n = 1$ `to` $nstep$ `do:`

Begin integration method update:

$\mathbf{e}_{in} \leftarrow \mathbf{e}^{n-1}$

$\mathbf{h}_{in} \leftarrow \mathbf{h}^{n-1}$

Update the electric and magnetic fields values:

`for` $j = 1$ `to` 4 `do`

$\mathbf{e}_{out} \leftarrow \mathbf{e}_{in} + \alpha_j \Delta t \mathbf{M}_\varepsilon^{-1}\left(\mathbf{G}^\top \mathbf{h}_{in} + \mathbf{j}^n\right)$

$\mathbf{h}_{out} \leftarrow \mathbf{h}_{in} + \beta_j \Delta t \mathbf{M}_\mu^{-1} \mathbf{G} \mathbf{e}_{out}$

$\mathbf{e}_{in} \leftarrow \mathbf{e}_{out}$

$\mathbf{h}_{in} \leftarrow \mathbf{h}_{out}$

`end for`

Update the electric and magnetic fields values for this time step:

$\mathbf{e}^n \leftarrow \mathbf{e}_{out}$

$\mathbf{h}^n \leftarrow \mathbf{h}_{out}$

`end for`

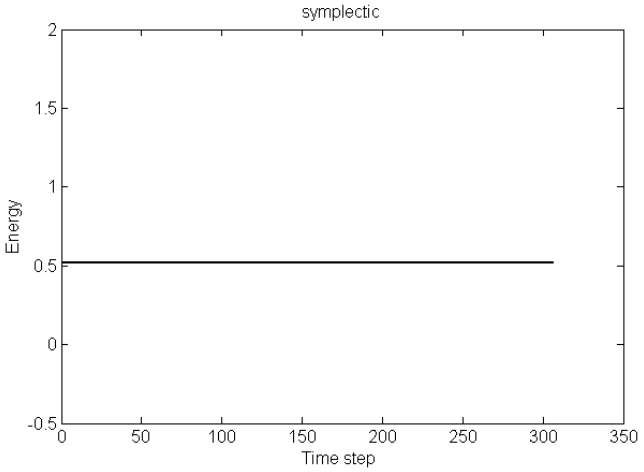

FIGURE 2. The energy of the system remains constant if the symplectic time integration method is applied.

Completion:

$\mathbf{e}^N \leftarrow \mathbf{e}^{nstep}$

$\mathbf{h}^N \leftarrow \mathbf{h}^{nstep}$

Krylov solvers were used to invert the mass matrices $\mathbf{M}_\varepsilon$ and $\mathbf{M}_\mu$. A preconditioned conjugate gradient solver was also implemented.

C. ENERGY CONSERVATION

In order to verify a correct physical behaviour of the numerical methods, we considered the energy evolution, too. The discrete instantaneous energy is the total energy that is stored in the discrete electric and magnetics fields. It is computed as

$$Energy = \frac{1}{2}\left(\mathbf{e}^T \mathbf{M}_\varepsilon \mathbf{e} + \mathbf{h}^T \mathbf{M}_\mu \mathbf{h}\right).$$

It is an substantial advantage of the symplectic method that it conserves the energy, see Fig. 2.

D. SIMULATION RESULTS, VALIDATIONS AND DISCUSSION

A number of numerical experiments were performed to approximate solutions of time dependent Maxwell's problems. We visualized the electromagnetic fields for cases where the exact solution is known, but also for cases with unknown analytical solution, and checked the stability and convergence properties in problems with complicated geometries. The main object of these simulations was to validate the code. The simulations are conditionally stable in the case of the symplectic time integration method.

EXAMPLE 1: This test example is characterized by the following parameters, where a symplectic time integration method is applied to a Fichera mesh. The frequency is $f = \frac{\sqrt{3}}{2} c_0$ Hz, where c_0 denotes the speed of light in vacuum, and the wave length is $\lambda = 1.1547$ m. The angular frequency is $\omega = 2\pi f$ (rad·s^{-1}). The permittivity and the permeability are equal to the constant vacuum values $\varepsilon = \varepsilon_0$ and $\mu = \mu_0$ as

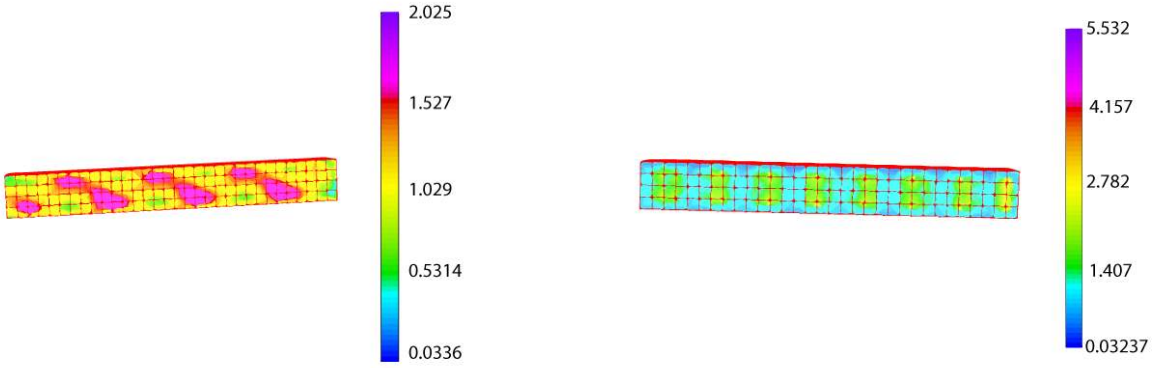

FIGURE 3. The snapshot is taken at the final time step ($N = 100$) for the electric and magnetic fields, by employing the backward Euler method for the beam tetrahedron. The time step size is $\Delta t = 0.03125$. (a) Electric field. (b) Magnetic field.

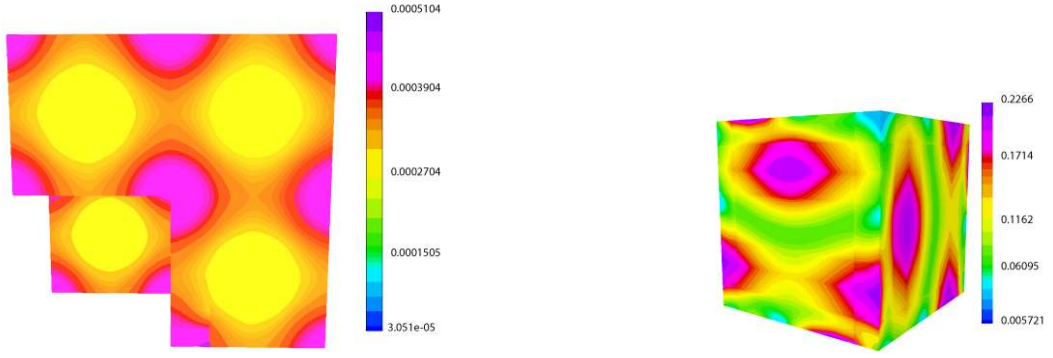

FIGURE 4. The snapshot is taken at the first time step ($n = 1$) for the electric and magnetic fields by taking the projections (31), and employing the backward Euler method for the Fichera mesh. The time step size is $\Delta t = 0.0005$. (a) Electric field. (b) Magnetic field.

in [83]. The exact electric and magnetic fields are given as

$$\begin{aligned}
\mathbf{E}_1(t) &= -\cos(\pi x)\sin(\pi y)\sin(\pi z)\cos(\omega t),\\
\mathbf{E}_2(t) &= 0,\\
\mathbf{E}_3(t) &= \sin(\pi x)\sin(\pi y)\cos(\pi z)\cos(\omega t),\\
\mathbf{H}_1(t) &= -\frac{\pi}{\omega}\sin(\pi x)\cos(\pi y)\cos(\pi z)\sin(\omega t),\\
\mathbf{H}_2(t) &= \frac{2\pi}{\omega}\cos(\pi x)\sin(\pi y)\cos(\pi z)\sin(\omega t),\\
\mathbf{H}_3(t) &= -\frac{\pi}{\omega}\cos(\pi x)\cos(\pi y)\sin(\pi z)\sin(\omega t).
\end{aligned}$$

For the case of the symplectic time integration method, an upper bound of the largest stable time step (CFL) is given by [2], [5], [81], as

$$\Delta t \leq \frac{2}{\sqrt{\rho\left(\mathbf{M}_\varepsilon^{-1}\mathbf{G}^\top\mathbf{M}_\mu^{-1}\mathbf{G}\right)}},$$

where ρ is the spectral radius function. The largest eigenvalue can be efficiently determined by [84] or the power method.

EXAMPLE 2: Here the backward Euler method is considered. The permittivity and the permeability are constant: $\varepsilon = 2$, $\mu = 1.5$. The initial electric and magnetic fields are obtained by taking the projections (31) of the exact electric and magnetic fields, where the exact fields given by

$$\begin{aligned}
\mathbf{E} &= \Big(\sin(2t-3z), \sin(2t-3x), \sin(2t-3y)\Big)^T,\\
\mathbf{H} &= \Big(\sin(2t-3y), \sin(2t-3z), \sin(2t-3x)\Big)^T,\\
\mathbf{J} &= \Big(\sin(2t-3z), \sin(2t-3x), \sin(2t-3y)\Big)^T.
\end{aligned}$$

Theorem 1 states that the problem is well-posed. An analogous result for the Rothe method is given in Theorem 2. The Theorems 3 and 4 present a priori estimates of the absolute error. These results show that we get optimal solutions within the selected finite element spaces, whereas many existing methods exhibit spurious solutions e.g. [1]–[15], [18], [27], [32], [34], [36] also because they solve other than the direct Maxwell's problem (1)-(3). We measured the $\mathbf{L}^2$-norm of the error for a sequence of successively refined meshes starting from a uniform coarse mesh. The refinement level at $l = 1$ shows the initial geometry of the mesh, and the levels at $l = 2, l = 3$, and $l = 4$ show the uniform refinement simultaneously at the subsequent 2nd, 3rd and 4th steps. We summarize the obtained absolute errors for the fourth

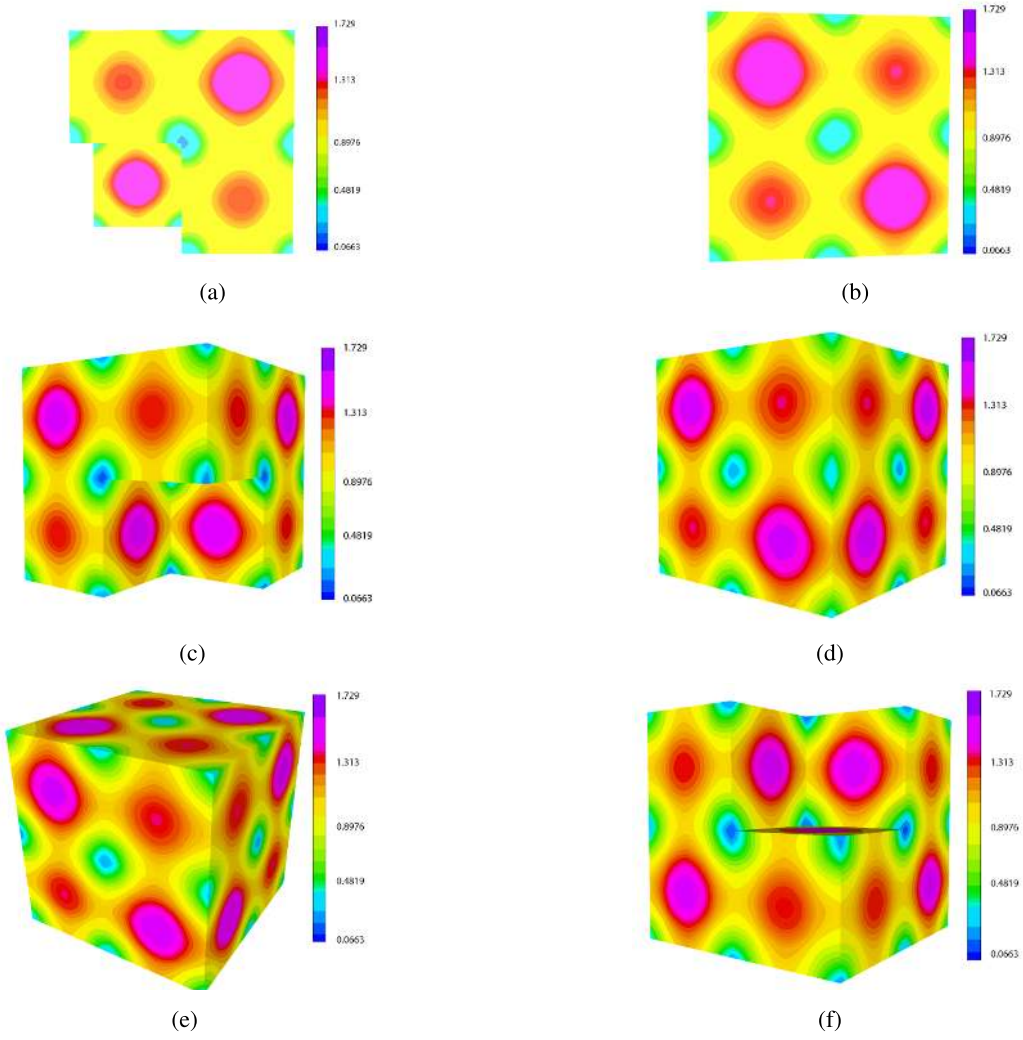

FIGURE 5. The scale shows the values of electric fields at the final time step ($N = 50$), by employing the backward Euler method. The time step size is $\Delta t = 0.0005$. (a) Snapshot of top. (b) Snapshot of bottom. (c) Snapshot of top and front. (d) Snapshot of back and bottom. (e) Snapshot of back, left and bottom. (f) Snapshot of right and front.

TABLE 1. Absolute error.

Refinement level	Electric and magnetic fields					
	$\|\mathbf{E}(t^n) - \mathbf{E}_h^n\|_{\mathbf{L}^2(\Omega)}$	order	$\|\mathbf{H}(t^n) - \mathbf{H}_h^n\|_{\mathbf{L}^2(\Omega)}$	order	stable time step Δt	Maximum number of steps
$l = 2$	0.584249		1.9114e-08		0.28230 ns	50
$l = 3$	0.041732	3.51	1.1946e-09	4.00	0.140619 ns	100
$l = 4$	0.002782	3.75	8.2386e-11	3.63	0.0706727 ns	250

order symplectic integration method in Table 1. The Table 1 shows that the symplectic method is conditionally stable and its order of the convergence is approximately equal to 4. Fig 2 illustrates that the symplectic method conserves the energy. This is an additional aspect to underline the good accuracy of our numerical results.

The snapshot of the electric and magnetic fields depicted in Fig. 3 is taken at the final time step $N = 100$, using the time step size $\Delta t = 0.03125$, by employing the backward Euler method for the beam tetrahedron meshes. Fig. 4 shows the initial values of the electric and magnetic fields at the first time step by taking the projections (31), and by employing the backward Euler method for the Fichera mesh (3D L-shaped domain). The time step size is $\Delta t = 0.0005$ in Fig. 4. Different orientations of the Fichera mesh are illustrated in Figs. 5. Furthermore, the electric and magnetic fields at time step $N = 50$ are shown in Fig. 5, by employing the backward Euler for $\Delta t = 0.0005$. Both the absolute errors and the conservation property of energy are determined and are strictly fulfilled as the electric and magnetic fields visualization in 3D underline for our cases, in contrast to [45]. This is clear from Table 1 and the conservation property of energy, see Fig. 2.

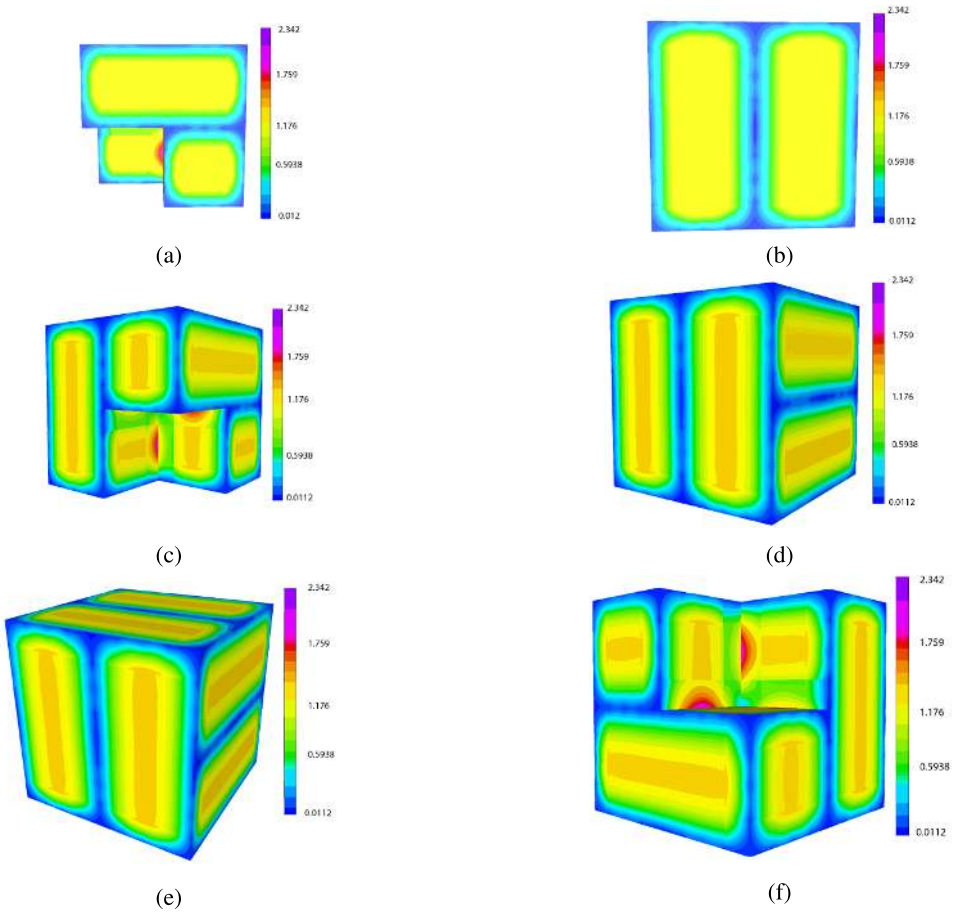

FIGURE 6. The scale shows the values of magnetic fields at the final time step ($N = 50$), by employing the backward Euler method. The time step size is $\Delta t = 0.0005$. (a) Snapshot of top. (b) Snapshot of bottom. (c) Snapshot of top and front. (d) Snapshot of back and bottom. (e) Snapshot of back, left and bottom. (f) Snapshot of right and front.

In addition, the electric and magnetic fields are visualized at initial and final time steps for beam and Fichera meshes.

The backward Euler method is unconditionally stable and computationally expensive. In contrast to the backward Euler method the symplectic method is conditionally stable. We conclude that our proposed time domain finite element method methods possess good accuracy and no spurious solutions in 3D complex geometries, and allow to treat the systems of Maxwell's equations directly and more efficiently than many existing methods such as A-formulation, $A - \Phi$ method, operator-form, electric field formulation, magnetic field formation and decoupled scheme (explicit magnetic field), for details see [1]–[15], [18], [27], [32], [34], [36]. Moreover the proposed methods are a good basis for the development of energy conserving methods for nonlinear problems in Optics and Photonics. The A-formulation scheme [9] also caused spurious solution in the nonlinear case. Moreover, our proposed method could replace the A-formulation [9] to solve the fully non-linear system of High-Power microwave air breakdown without spurious solutions. We have also obtained some first parallel results, see [85].

VII. CONCLUSION

The paper summarizes some time domain finite element methods for the system of Maxwell's equations in three dimensions, where the electric and magnetic fields are discretized by means of different finite element spaces. The time domain mixed finite element methods have the advantage of being substantially more powerful and reliable than FDTD or other existing methods with respect to error estimates and numerical experiment, because they directly solve the system for electric and magnetic field intensities. Moreover the Rothe method and fully-discrete error estimation yield optimal solutions. To the best of our knowledge, fully discrete error estimates, simulations and visualizations of the type presented here, using the Nédeléc curl-conforming and Raviart Thomas div-conforming elements with backward Euler temporal discretization for the system of Maxwell's equations, were not yet available. Numerical examples are given for the fully discrete problems.

The presented symplectic time integration method is accurate up to fourth order in time, conserves the energy and is conditionally stable. The backward Euler method is

unconditionally stable. The computed electric and magnetic fields are visualized at intermediate and final time steps.

APPENDIX
SOME INEQUALITIES

Lemma 1: Let X be a real Hilbert space with inner product $(\cdot,\cdot)$. Then the following relations are valid for all $\mathbf{u},\mathbf{v}\in X$:

1) $2(\mathbf{u}-\mathbf{v},\mathbf{u}) = \|\mathbf{u}\|^2 + \|\mathbf{u}-\mathbf{v}\|^2 - \|\mathbf{v}\|^2$,
2) $|(\mathbf{u},\mathbf{v})| \le \frac{\alpha}{2}\|\mathbf{u}\|^2 + \frac{1}{2\alpha}\|\mathbf{v}\|^2$ *for all* $\alpha > 0$.

Proof: (1) follows from

$$\begin{aligned}\|\mathbf{v}\|^2 &= (\mathbf{v}-\mathbf{u}+\mathbf{u},\mathbf{v}-\mathbf{u}+\mathbf{u})\\ &= \|\mathbf{v}-\mathbf{u}\|^2 + 2(\mathbf{v}-\mathbf{u},\mathbf{u}) + \|\mathbf{u}\|^2\\ &= \|\mathbf{u}-\mathbf{v}\|^2 - 2(\mathbf{u}-\mathbf{v},\mathbf{u}) + \|\mathbf{u}\|^2.\end{aligned}$$

(2) Obviously, $0 \le \|\mathbf{u}\pm\mathbf{v}\|^2 \le \|\mathbf{u}\|^2 \pm 2(\mathbf{u},\mathbf{v}) + \|\mathbf{v}\|^2$, hence $2|(\mathbf{u},\mathbf{v})| \le \|\mathbf{u}\|^2 + \|\mathbf{v}\|^2$.

Replacing in this inequality $\mathbf{u}$ by $\sqrt{\alpha}\mathbf{u}$ and $\mathbf{v}$ by $\mathbf{v}/\sqrt{\alpha}$, the statement follows. □

Lemma 2: Let $\delta \ge 0$, $g_0 \ge 0$ and (a_n), (b_n), (c_n) and (γ_n) be sequences of nonnegative numbers such that

$$a_n + \delta\sum_{j=0}^{n} b_j \le \delta\sum_{j=0}^{n}\gamma_j a_j + \delta\sum_{j=0}^{n} c_j + g_0 \quad \text{for all } n = 0,1,2\ldots \tag{34}$$

Assume that $\gamma_j\delta < 1$ for all j, and set $\sigma_j := (1-\gamma_j\delta)^{-1}$. Then it holds, for all $n \ge 0$:

$$a_n + \delta\sum_{j=0}^{n} b_j \le \left(\delta\sum_{j=0}^{n} c_j + g_0\right)\exp\left(\delta\sum_{j=0}^{n}\sigma_j\gamma_j\right).$$

Proof: Since the assumption (34) can be rewritten as

$$(1-\gamma_n\delta)a_n + \delta\sum_{j=0}^{n} b_j \le \delta\sum_{j=0}^{n-1}\gamma_j a_j + \delta\sum_{j=0}^{n} c_j + g_0,$$

it takes – after some further simple manipulations – a form as assumed in [86, Lemma 2.1], and the results follows from that Lemma. □

ACKNOWLEDGMENT

The authors would like to thank the anonymous reviewers for their helpful and constructive comments that greatly contributed to improving the final version of the paper. We would also like to thank the Associate Editor for the generous comments and support during the review process.

REFERENCES

[1] P. Monk, "Analysis of a finite element method for Maxwell's equations," *SIAM J. Numer. Anal.*, vol. 29, no. 3, pp. 714–729, Jun. 1992.
[2] J.-F. Lee, R. Lee, and A. Cangellaris, "Time-domain finite-element methods," *IEEE Trans. Antennas Propag.*, vol. 45, no. 3, pp. 430–442, May 1997.
[3] P. Neittaanmäki and J. Saranen, "Semi-discrete Galerkin approximation method applied to initial boundary value problems for Maxwell's equations in anisotropic, inhomogeneous media," *Proc. Roy. Soc. Edinburgh Sect. A, Math.*, vol. 89, nos. 1–2, pp. 125–133, 1981.
[4] P. Ciarlet, Jr., and L. Zou, "Fully discrete finite element approaches for time-dependent Maxwell's equations," *Numerische Mathematik*, vol. 82, no. 2, pp. 193–219, Apr. 1999.
[5] D. A. White and M. Stowell, "Full-wave simulation of electromagnetic coupling effects in RF and mixed-signal ICs using a time-domain finite-element method," *IEEE Trans. Microw. Theory Techn.*, vol. 52, no. 5, pp. 1404–1413, May 2004.
[6] W. A. Artuzi, "Improving the Newmark time integration scheme in finite element time domain methods," *IEEE Microw. Wireless Compon. Lett.*, vol. 15, no. 12, pp. 898–900, Dec. 2005.
[7] M. Hochbruck and C. Stohrer, "Finite element heterogeneous multiscale method for time-dependent Maxwell's equations," in *Proc. Spectral High Order Methods Partial Differ. Equ. (ICOSAHOM)*. Rio de Janeiro, Brazil: Springer, Aug. 2017, pp. 269–281.
[8] A. Akbarzadeh-Sharbaf and D. D. Giannacopoulos, "A stable and efficient direct time integration of the vector wave equation in the finite-element time-domain method for dispersive media," *IEEE Trans. Antennas Propag.*, vol. 63, no. 1, pp. 314–321, Jan. 2015.
[9] S. Yan and J.-M. Jin, "A fully coupled nonlinear scheme for time-domain modeling of high-power microwave air breakdown," *IEEE Trans. Microw. Theory Techn.*, vol. 64, no. 9, pp. 2718–2729, Sep. 2016.
[10] N. Liu, G. Cai, C. Zhu, Y. Huang, and Q. H. Liu, "The mixed finite-element method with mass lumping for computing optical waveguide modes," *IEEE J. Sel. Topics Quantum Electron.*, vol. 22, no. 2, Mar./Apr. 2016, Art. no. 4400709.
[11] J. Diaz and M. J. Grote, "Multi-level explicit local time-stepping methods for second-order wave equations," *Comput. Methods Appl. Mech. Eng.*, vol. 291, pp. 240–265, Jul. 2015.
[12] S. Ho, Y. Zhao, W. N. Fu, and P. Zhou, "Application of edge elements to 3-D electromagnetic field analysis accounting for both inductive and capacitive effects," *IEEE Trans. Magn.*, vol. 52, no. 3, Mar. 2016, Art. no. 7400504.
[13] J. Li, X. Lu, C. G. Farquharson, and X. Hu, "A finite-element time-domain forward solver for electromagnetic methods with complex-shaped loop sources," *Geophysics*, vol. 83, no. 3, pp. E117–E132, May 2018.
[14] M. J. Grote, M. Mehlin, and T. Mitkova, "Runge–Kutta-based explicit local time-stepping methods for wave propagation," *SIAM J. Sci. Comput.*, vol. 37, no. 2, pp. A747–A775, 2015.
[15] J. Bai, Y. Cao, X. He, H. Liu, and X. Yang, "Modeling and an immersed finite element method for an interface wave equation," *Comput. Math. Appl.*, vol. 76, no. 7, pp. 1625–1638, Oct. 2018.
[16] P. B. Monk, "A mixed method for approximating Maxwell's equations," *SIAM J. Numer. Anal.*, vol. 28, no. 6, pp. 1610–1634, 1991.
[17] P. Monk, "An analysis of Nédélec's method for the spatial discretization of Maxwell's equations," *J. Comput. Appl. Math.*, vol. 47, no. 1, pp. 101–121, Jun. 1993.
[18] C. Makridakis and P. Monk, "Time-discrete finite element schemes for Maxwell's equations," *ESAIM: Math. Model. Numer. Anal.*, vol. 29, no. 2, pp. 171–197, 1995.
[19] J.-M. Jin, M. Zunoubi, K. C. Donepudi, and W. C. Chew, "Frequency-domain and time-domain finite-element solution of Maxwell's equations using spectral Lanczos decomposition method," *Comput. Methods Appl. Mech. Eng.*, vol. 169, nos. 3–4, pp. 279–296, Feb. 1999.
[20] R. L. Lee and N. K. Madsen, "A mixed finite element formulation for Maxwell's equations in the time domain," *J. Comput. Phys.*, vol. 88, no. 2, pp. 284–304, Jun. 1990.
[21] G. Rodrigue and D. White, "A vector finite element time-domain method for solving Maxwell's equations on unstructured hexahedral grids," *SIAM J. Sci. Comput.*, vol. 23, no. 3, pp. 683–706, 2001.
[22] J. Li, "Error analysis of fully discrete mixed finite element schemes for 3-D Maxwell's equations in dispersive media," *Comput. Methods Appl. Mech. Eng.*, vol. 196, nos. 33–34, pp. 3081–3094, Jul. 2007.
[23] J. Li, "Error analysis of mixed finite element methods for wave propagation in double negative metamaterials," *J. Comput. Appl. Math.*, vol. 209, no. 1, pp. 81–96, Dec. 2007.
[24] D. Jiao and J.-M. Jin, "A general approach for the stability analysis of the time-domain finite-element method for electromagnetic simulations," *IEEE Trans. Antennas Propag.*, vol. 50, no. 11, pp. 1624–1632, Nov. 2002.
[25] J.-F. Lee and Z. Sacks, "Whitney elements time domain (WETD) methods," *IEEE Trans. Magn.*, vol. 31, no. 3, pp. 1325–1329, May 1995.

[26] J. Zhao, "Analysis of finite element approximation for time-dependent Maxwell problems," *Math. Comput.*, vol. 73, no. 247, pp. 1089–1105, 2004.
[27] C. Ma, "Finite-element method for time-dependent Maxwell's equations based on an explicit-magnetic-field scheme," *J. Comput. Appl. Math.*, vol. 194, no. 2, pp. 409–424, Oct. 2006.
[28] F. L. Teixeira, "Time-domain finite-difference and finite-element methods for Maxwell equations in complex media," *IEEE Trans. Antennas Propag.*, vol. 56, no. 8, pp. 2150–2166, Aug. 2008.
[29] Y. Zhang, L.-Q. Cao, and Y.-S. Wong, "Multiscale computations for 3D time-dependent Maxwell's equations in composite materials," *SIAM J. Sci. Comput.*, vol. 32, no. 5, pp. 2560–2583, 2010.
[30] J. Kim and F. L. Teixeira, "Parallel and explicit finite-element time-domain method for Maxwell's equations," *IEEE Trans. Antennas Propag.*, vol. 59, no. 6, pp. 2350–2356, Jun. 2011.
[31] W. Yang, Y. Huang, and J. Li, "Developing a time-domain finite element method for the Lorentz metamaterial model and applications," *J. Sci. Comput.*, vol. 68, no. 2, pp. 438–463, Aug. 2016.
[32] A. Anees and L. Angermann, "Mixed finite element methods for the Maxwell's equations with matrix parameters," in *Proc. Int. Appl. Comput. Electromagn. Soc. Symp. (ACES)*, Mar. 2018, pp. 1–2.
[33] Y. Huang, J. Li, and Q. Lin, "Superconvergence analysis for time-dependent Maxwell's equations in metamaterials," *Numer. Methods Partial Differ. Equ.*, vol. 28, no. 6, pp. 1794–1816, Nov. 2012.
[34] J. Li and Y. Lin, "A priori and posteriori error analysis for time-dependent Maxwell's equations," *Comput. Methods Appl. Mech. Eng.*, vol. 292, pp. 54–68, Aug. 2015.
[35] A. Anees and L. Angermann, "Time domain finite element methods for Maxwell's equations in three dimensions," in *Proc. Int. Appl. Comput. Electromagn. Soc. Symp. (ACES)*, Mar. 2018, pp. 1–2.
[36] A. Anees and L. Angermann, "A mixed finite element methods approximation for the Maxwell's equations in electromagnetics," in *Proc. IEEE/ACES Int. Conf. Wireless Inf. Technol. Syst. (ICWITS) Appl. Comput. Electromagn. (ACES)*, Mar. 2016, pp. 1–2.
[37] J. Cai, J. Hong, Y. Wang, and Y. Gong, "Two energy-conserved splitting methods for three-dimensional time-domain Maxwell's equations and the convergence analysis," *SIAM J. Numer. Anal.*, vol. 53, no. 4, pp. 1918–1940, 2015.
[38] R. Abedi and S. Mudaliar, "An asynchronous spacetime discontinuous Galerkin finite element method for time domain electromagnetics," *J. Comput. Phys.*, vol. 351, pp. 121–144, Dec. 2017. [Online]. Available: http://www.sciencedirect.com/science/article/pii/S0021999117306514
[39] M. Dawson, R. Seville, and K. Morgan, "The application of a high-order discontinuous Galerkin time-domain method for the computation of electromagnetic resonant modes," *Appl. Math. Model.*, vol. 55, pp. 94–108, Mar. 2018.
[40] E. T. Chung and B. Engquist, "Optimal discontinuous Galerkin methods for wave propagation," *SIAM J. Numer. Anal.*, vol. 44, no. 5, pp. 2131–2158, 2006.
[41] V. Dolean, S. Lanteri, and R. Perrussel, "A domain decomposition method for solving the three-dimensional time-harmonic Maxwell equations discretized by discontinuous Galerkin methods," *J. Comput. Phys.*, vol. 227, no. 3, pp. 2044–2072, Jan. 2008.
[42] H. Fahs, "High-order discontinuous Galerkin method for time-domain electromagnetics on non-conforming hybrid meshes," *Math. Comput. Simul.*, vol. 107, pp. 134–156, Jan. 2015.
[43] M. J. Grote and T. Mitkova, "Explicit local time-stepping methods for Maxwellâ Źs equations," *J. Comput. Appl. Math.*, vol. 234, no. 12, pp. 3283–3302, Oct. 2010.
[44] J. Li, C. Shi, and C.-W. Shu, "Optimal non-dissipative discontinuous Galerkin methods for Maxwell's equations in Drude metamaterials," *Comput. Math. Appl.*, vol. 73, no. 8, pp. 1760–1780, Apr. 2017.
[45] C. Shi, J. Li, and C.-W. Shu, "Discontinuous Galerkin methods for Maxwell's equations in Drude metamaterials on unstructured meshes," *J. Comput. Appl. Math.*, vol. 342, pp. 147–163, Nov. 2018.
[46] S. Shields, J. Li, and E. A. Machorro, "Weak Galerkin methods for time-dependent Maxwell's equations," *Comput. Math. Appl.*, vol. 74, no. 9, pp. 2106–2124, Nov. 2017.
[47] D. Sármány, M. A. Botchev, and J. J. van der Vegt, "Time-integration methods for finite element discretisations of the second-order Maxwell equation," *Comput. Math. Appl.*, vol. 65, no. 3, pp. 528–543, Feb. 2013.
[48] B. Wang, Z. Xie, and Z. Zhang, "Space-time discontinuous Galerkin method for Maxwell equations in dispersive media," *Acta Math. Scientia*, vol. 34, no. 5, pp. 1357–1376, Sep. 2014.
[49] M. Hochbruck and T. Pažur, "Implicit Runge–Kutta methods and discontinuous Galerkin discretizations for linear Maxwell's equations," *SIAM J. Numer. Anal.*, vol. 53, no. 1, pp. 485–507, 2015.
[50] M. Dehghan and R. Salehi, "A meshless local Petrov–Galerkin method for the time-dependent Maxwell equations," *J. Comput. Appl. Math.*, vol. 268, pp. 93–110, Oct. 2014.
[51] P. Monk and E. Süli, "A convergence analysis of Yee's scheme on nonuniform grids," *SIAM J. Numer. Anal.*, vol. 31, no. 2, pp. 393–412, 1994.
[52] T. Kang, K. Van Bockstal, and R. Wang, "The reconstruction of a time-dependent source from a surface measurement for full Maxwell's equations by means of the potential field method," *Comput. Math. Appl.*, vol. 75, no. 3, pp. 764–786, Feb. 2018.
[53] P. Monk, "A comparison of three mixed methods for the time-dependent Maxwell's equations," *SIAM J. Sci. Stat. Comput.*, vol. 13, no. 5, pp. 1097–1122, 1992.
[54] R. Hiptmair, "Finite elements in computational electromagnetism," *Acta Numer.*, vol. 11, pp. 237–339, Jan. 2002.
[55] S. Labbé, "Fast computation for large magnetostatic systems adapted for micromagnetism," *SIAM J. Sci. Comput.*, vol. 26, no. 6, pp. 2160–2175, 2005.
[56] H. Fu *et al.*, "A parallel finite-element time-domain method for transient electromagnetic simulation," *Geophysics*, vol. 80, no. 4, pp. E213–E224, Jul. 2015.
[57] L. D. Angulo, J. Alvarez, F. L. Teixeira, M. F. Pantoja, and S. G. Garcia, "A nodal continuous-discontinuous Galerkin time-domain method for Maxwell's equations," *IEEE Trans. Microw. Theory Techn.*, vol. 63, no. 10, pp. 3081–3093, Oct. 2015.
[58] K. S. Atia, A. Heikal, and S. S. A. Obayya, "Efficient smoothed finite element time domain analysis for photonic devices," *Opt. Express*, vol. 23, no. 17, pp. 22199–22213, Aug. 2015.
[59] M. C. Pinto, M. Mounier, and E. Sonnendrücker, "Handling the divergence constraints in Maxwell and Vlasov–Maxwell simulations," *Appl. Math. Comput.*, vol. 272, pp. 403–419, Jan. 2016.
[60] Y. Shao, J. J. Yang, and M. Huang, "A review of computational electromagnetic methods for graphene modeling," *Int. J. Antennas Propag.*, vol. 2016, Apr. 2016, Art. no. 7478621.
[61] H. Cai, X. Hu, J. Li, M. Endo, and B. Xiong, "Parallelized 3D CSEM modeling using edge-based finite element with total field formulation and unstructured mesh," *Comput. Geosci.*, vol. 99, pp. 125–134, Feb. 2017.
[62] J. Zheng, H. Huang, S. Zhang, and Z. Deng, "A general method to simulate the electromagnetic characteristics of HTS Maglev systems by finite element software," *IEEE Trans. Appl. Supercond.*, vol. 28, no. 5, Aug. 2018, Art. no. 3600808.
[63] J.-M. Jin, *The Finite Element Method in Electromagnetics*. Hoboken, NJ, USA: Wiley, 2015.
[64] J. Li and Y. Huang, *Time-Domain Finite Element Methods for Maxwell's Equations in Metamaterials*, vol. 43. New York, NY, USA: Springer, 2012.
[65] P. Monk, *Finite Element Methods for Maxwell's Equations*. New York, NY, USA: Oxford Univ. Press, 2003.
[66] D. B. Davidson, *Computational Electromagnetics for RF and Microwave Engineering*. Cambridge, U.K.: Cambridge Univ. Press, 2010.
[67] S. R. H. Hoole, *Finite Elements, Electromagnetics and Design*. Amsterdam, The Netherlands: Elsevier, 1995.
[68] L. Angermann and V. V. Yatsyk, *Resonant Scattering and Generation of Waves: Cubically Polarizable Layers*. Cham, Switzerland: Springer, 2018.
[69] A. Bossavit, "Whitney forms: A class of finite elements for three-dimensional computations in electromagnetism," *IEE A, Phys. Sci., Meas. Instrum., Manage. Educ., Rev.*, vol. 135, no. 8, pp. 493–500, Nov. 1988.
[70] A. Bossavit, "Solving Maxwell equations in a closed cavity, and the question of 'spurious modes'," *IEEE Trans. Magn.*, vol. 26, no. 2, pp. 702–705, Mar. 1990.
[71] J. C. Nédélec, "Mixed finite elements in R^3," *Numerische Mathematik*, vol. 35, no. 3, pp. 315–341, Sep. 1980.
[72] J. C. Nédélec, "A new family of mixed finite elements in R^3," *Numerische Mathematik*, vol. 50, no. 1, pp. 57–81, Jan. 1986.

[73] P.-A. Raviart and J. M. Thomas, "A mixed finite element method for 2-nd order elliptic problems," in *Mathematical Aspects of Finite Element Methods*. Berlin, Germany: Springer, 1977, pp. 292–315.
[74] R. Leis, *Initial Boundary Value Problems in Mathematical Physics*. Hoboken, NJ, USA: Wiley, 1988.
[75] J. Lions and G. Duvaut, *Inequalities in Mechanics and Physics*. Berlin, Germany: Springer, 1976.
[76] A. Kufner, O. John, and S. Fucik, *Function spaces*. Prague, Czech Republic: Academic, 1977.
[77] R. Adams and J. Fournier, "Sobolev spaces," in *Pure and Applied Mathematics* (Amsterdam), vol. 140, 2nd ed. Amsterdam, The Netherlands: Elsevier, 2003.
[78] V. Girault and P. Raviart, *Finite Element Methods for Navier-Stokes Equations: Theory and Algorithms*. New York, NY, USA: Springer-Verlag, 1986.
[79] P. G. Ciarlet, *The Finite Element Method for Elliptic Problems*. Philadelphia, PA, USA: SIAM, 2002.
[80] B. G. Pachpatte, "On a certain inequality arising in the theory of differential equations," *J. Math. Anal. Appl.*, vol. 182, no. 1, pp. 143–157, Feb. 1994.
[81] A. Fisher, D. White, and G. Rodrigue, "An efficient vector finite element method for nonlinear electromagnetic modeling," *J. Comput. Phys.*, vol. 225, no. 2, pp. 1331–1346, 2007.
[82] R. Rieben, D. White, and G. Rodrigue, "High-order symplectic integration methods for finite element solutions to time dependent Maxwell equations," *IEEE Trans. Antennas Propag.*, vol. 52, no. 8, pp. 2190–2195, Aug. 2004.
[83] A. Christophe, S. Descombes, and S. Lanteri, "An implicit hybridized discontinuous Galerkin method for the 3D time-domain Maxwell equations," *Appl. Math. Comput.*, vol. 319, pp. 395–408, Feb. 2015.
[84] W. E. Arnoldi, "The principle of minimized iterations in the solution of the matrix eigenvalue problem," *Quart. Appl. Math.*, vol. 9, no. 1, pp. 17–29, 1951.
[85] A. Anees and L. Angermann, "Time domain finite element methods for Maxwell's equations," in *Proc. 7th Workshop Parallel-in-Time Methods*, Roscoff Marine station. Roscoff, France, May 2018, pp. 1–32. [Online]. Available: http://www.math.univ-paris13.fr/~japhet/PINT/Slides/Asad_ANEES_PinT2018.pdf
[86] A. Quarteroni and A. Valli, *Numerical Methods for Partial Differential Equations*. New York, NY, USA: Springer, 1994.

ASAD ANEES received the M.Sc. degree in applied mathematics from the University of Engineering and Technology at Lahore, Lahore, Pakistan, in 2009. He is currently pursuing the Ph.D. degree in applied mathematics with the Institute of Mathematics, Clausthal University of Technology, Germany, where he is also a Member of a research project.

Since 2011, he has been a tenured Lecturer in mathematics with the Department of Mathematics and Statistics, University of Agriculture Faisalabad, Punjab, Pakistan. He has been having two positions, since 2014. His current research interests include high performance computing, space-time parallel method, error estimation, and scientific visualization for electromagnetic and nonlinear optics. In particular, his expertise includes the development of theoretical aspects of higher order spatial, temporal discretization, and energy conserving time domain finite element methods (TDFEM) with nonlinear material in computational electromagnetic and optics.

LUTZ ANGERMANN received the Ph.D. degree from the University of Technology at Dresden, in 1987, and the Habilitation degree from the University of Erlangen-Nürnberg, in 1995. He studied Mathematics with the State University of Kharkiv (now V. N. Karazin Kharkiv National University, Ukraine).

From 1998 to 2001, he was an Associate Professor of numerical mathematics with the University of Magdeburg. Since 2001, he has been a Professor of numerical mathematics with the Department of Mathematics, Clausthal University of Technology. He has authored or coauthored about 120 scientific papers and four books among them. His research interest includes the mathematical analysis of numerical algorithms for partial differential equations with special interests in finite volume and finite element methods and their application to problems in physics and engineering.